FACULTY OF MEDICINE AND HEALTH SCIENCES

CHEMOGENETIC AND OPTOGENETIC MODULATION OF NORADRENERGIC NEURONS OF THE LOCUS COERULEUS IN THE RAT

Jeroen Spanoghe
Student number: 01410100

Supervisor(s): Prof. Dr. Robrecht Raedt, Prof. Dr. Kristl Vonck

A dissertation submitted to Ghent University in partial fulfilment of the requirements for the degree of Master of Science in the Biomedical Sciences

Academic year: 2018 - 2019

GHENT UNIVERSITY

Preface

I would like to thank everyone that helped me during the process of this Master's Dissertation. Learning and working at the 4Brain research laboratory for my thesis was an amazing experience because of all these people.

First of all I would like to thank Prof. Dr. Robrecht Raedt, my promotor, for his guidance and advice on the experiments I was able to perform in his laboratory. I would like to thank Wouter Van Lysebettens, my official mentor who helped with planning of the experiments and taught me several things despite being very busy himself with the finalization of his PhD. And I especially want to express my thanks to Latoya Stevens, under whose excellent mentorship I performed most of the work for my thesis. She taught me most of all the experimental techniques that I needed to perform and guided me extremely well in the writing of this dissertation. I would also like to thank all the other PhD students from the 4Brain group, on whose help I could always count, and my fellow master students in the lab.

And finally, I would like to thank my family and friends for their invaluable support outside of the lab.

Table of Contents

Summary

Background: The locus coeruleus (LC) has been attributed an important role in the anticonvulsive effects of vagus nerve stimulation (VNS). This therapy has been shown to cause changes in hippocampal excitability, which could possibly be partly mediated by norepinephrine (NE) released from the LC. However, it has also been shown that VNS induces hypothermia, a confounding factor. The goal of this project is to examine the effects of the LC-NE system on hippocampal excitability directly by activating the LC using chemo- or optogenetics.
Methods: Optogenetic modulation of the LC was pursued by stereotaxic injection of the CAV2-PRSx8-ChR2-mCherry vector. Opsin expression was evaluated by immunohistochemical double staining. Expression levels were quantified by determining ratios between the two fluorescence signals and by performing manual cell counts on confocal images.
Results: In a pilot trial with 3 animals, all injections resulted in successful LC transduction. In the following experiments, results were more variable. In the first set of unilateral injections, only 2 out of 6 injections resulted in successful transductions. In the second set of bilateral injections, 5 out of 8 injections produced satisfactory expression levels.
Conclusion: The overall success rate for LC transduction via stereotaxic injection in this project was 50%. This is a moderate amount, but not uncommon because of the difficulty inherent to targeting the LC. The injection procedure could use some further optimization to increase the success rate. For the quantification of expression levels, cell counting on confocal images has been shown to be the optimal approach.

1. Introduction

1.1 Epilepsy

Epilepsy is a chronic disease of the brain which affects approximately 50 million people worldwide, making it one of the most common neurological disorders [1]. It is defined as a chronic disease characterized by the generation of recurrent, unprovoked seizures. A seizure is a transient occurrence of symptoms caused by excessive, synchronous firing of neurons in the brain. The official classification of epileptic seizures is defined by the International League Against Epilepsy (ILAE) [2]. Seizures are classified into 3 categories based on the location of onset: generalized seizures, focal seizures and seizures with unknown onset. Generalized seizures involve abnormal neuronal firing originating in both cerebral hemispheres, while focal seizures start in only one of the hemispheres. If focal seizures propagate to both hemispheres, the term 'bilateral' is used. These categories can be further divided into subtypes based on the presence of motor or non-motor symptoms, and in case of focal onset seizures based on the presence of impaired awareness. The cause of these epileptic seizures lies in an imbalance between excitation and inhibition of neurons. The disruption of this balance can have a genetic origin or be due to acquired cerebral damage, with effects on the level of neuronal circuits, on receptors, on signaling cascades or on ion channel function [3].

The exact epidemiology of epilepsy is somewhat hindered by methodological problems such as diagnostic accuracy and case ascertainment., which leaves us only estimates of epidemiological data. The prevalence of active epilepsy is generally accepted to be between 5 and 10 cases per 1000 people. The incidence has been estimated to be around 50 per 100.000/year, but in resource-poor countries this number is likely higher [4].

For this large number of people suffering from epilepsy, first-line treatment exists of drugs designed to decrease electrical activity of neurons. This can be done by preventing depolarization (e.g. by blocking sodium/calcium channels or enhancing the activity of potassium channels), by inhibiting glutamergic excitation or by promoting GABAergic inhibition. The majority of people who suffer from epilepsy can effectively be treated with anti-epileptic drugs, but approximately 1/3 of the patients develop seizures that do not respond to this medication, called refractory epilepsy [5]. For these patients, several non-pharmacologic therapies exist. If the epileptic focus can clearly be located, resective surgery may be performed to remove the brain structure which causes the seizures. If this is not the case, other options such as a ketogenic diet or stimulation therapies could be indicated.

1.2 Vagus Nerve Stimulation

One of the available stimulation therapies is vagus nerve stimulation (VNS). This is a neuromodulatory treatment which consists of electrical stimulation of the 10th cranial nerve to produce anticonvulsive effects. The main therapeutic use of VNS is for the treatment of refractory epilepsy. However, VNS has also been approved for treating major depression and is under investigation for use in other disorders in which positive effects have been observed such as migraine, Alzheimer's disease and several psychiatric disorders [6, 7].

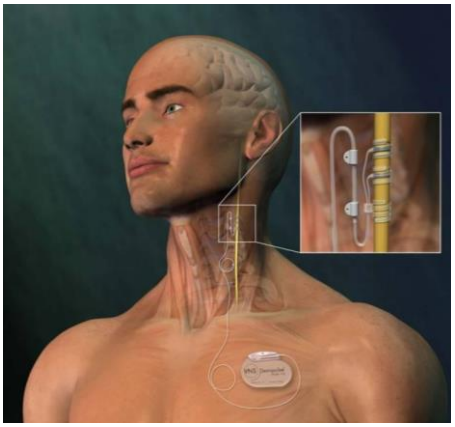

Fig. 1 Placement of VNS device and connection to the left vagus nerve. *Figure from Ekmekci H (2017)* [8]

The classical therapy requires surgical implantation of a pulse generator that is placed subcutaneously in the left chest. This generator is connected with a lead wire to helical electrodes placed around the left vagus nerve through which the generator sends electrical pulses to the nerve **(Fig. 1)**. Stimulation is normally always performed on the left side, as stimulation of the right vagus nerve could cause cardiac side effects [9]. The generator delivers pulses with programmable settings with a standard duty cycle of 30s ON/ 300s OFF and a stimulation amplitude of 0.5-3.5 milliamperes at a frequency of 20-30 Hertz [10]. Newer non-invasive VNS systems have also been developed to avoid adverse events related to implantation, such as transcutaneous VNS where the auricular branch of the vagus nerve is stimulated [11].

The vagus nerve is the longest cranial nerve starting from the medulla and reaching all the way down into the abdomen. It is composed of somatic and visceral afferent fibers (80%) and of visceral efferent fibers (20%). Efferent fibers originating from the dorsal motor nucleus X provide the parasympathetic innervation of thoracic and abdominal organs, while efferent fibers from the nucleus ambiguus are responsible for motor innervation of the pharynx and the larynx [12]. Most of the afferent fibers of the vagus nerve project to the sensory nucleus of the solitary tract (NST) in the medulla. The NST itself has efferent projections to many areas in the brain, including the amygdala, thalamus, hypothalamus, cerebellum, parabrachial nucleus, raphe nuclei and the locus coeruleus (LC) [13].

The first time a VNS device was implanted in a human to treat refractory epilepsy was in 1988. After several clinical studies, VNS has been approved and widely used since 1994 in Europe and since 1997 in the USA [12]. The efficacy of VNS has been demonstrated in several clinical studies, showing that on average 60% of the patients had a seizure reduction of at least 50% (responders) [12, 14]. However, the underlying physiological mechanism causing this reduction in seizures after electrical stimulation of the vagus nerve is not yet fully understood. Since the NST receives most of the vagal input, it is assumed that this structure and the nuclei downstream of it are responsible for the anticonvulsive effects of VNS. One such nucleus, the LC, has been ascribed an important role in these effects based on several studies.

1.3 Locus Coeruleus

The LC is a small nucleus in the pontine brainstem which is entirely composed of norepinephrine (NE)-containing neurons. Despite its small size, the LC is the major source of the modulatory neurotransmitter NE in the entire central nervous system (CNS) due to its widespread efferent projections **(Fig. 2)**. This LC-NE system modulates several behavioral functions and is important in the processing of salient information.

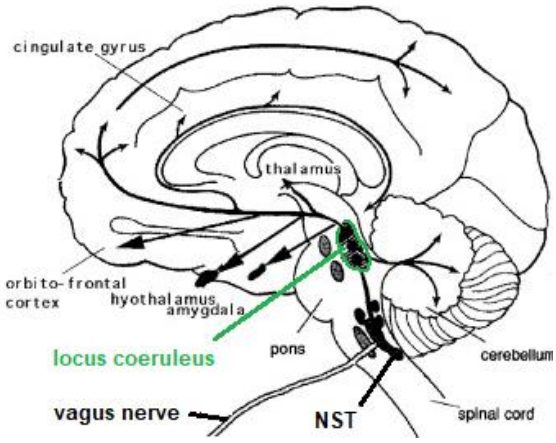

Fig. 2 Sagittal section of the brain illustrating the location of the locus coeruleus in the brainstem, its efferent projections and its connections with the vagus nerve and the nucleus of the solitary tract (NST).
Figure adapted from George MS (2004) [15]

1.3.1 Anatomy

The LC is positioned bilaterally in the brainstem adjacent to the fourth ventricle. Each nucleus contains around 1500 neurons in rodents, approximately 10.000-15.000 neurons in humans [16]. These neurons send out an extensive network of projections innervating the cerebrum, cerebellum, midbrain and spinal cord. The only structures of the CNS that do not receive LC projections are the basal ganglia. The widespread axons of LC neurons allow the LC to exert its effects all throughout the CNS with the volume transmission of the neuromodulator NE. Norepinephrine is synthesized in noradrenergic neurons from the amino acid tyrosine **(Fig. 3)**. The enzyme tyrosine hydroxylase (TH) converts tyrosine to L-DOPA, the precursor to dopamine. L-DOPA is converted to dopamine by DOPA decarboxylase (DDC). The conversion of dopamine to NE is then catalyzed by dopamine β-hydroxylase (DBH). All LC neurons produce NE, which initially led to the belief that it is a homogeneous structure composed of one type of neuron. However, studies have shown that the LC possesses heterogeneity on multiple levels. First of all, two types of noradrenergic cells have been distinguished: large multipolar cells and smaller fusiform cells [17]. Besides these morphological differences, there is also a distinction between neurons based on the expression of neuropeptides. All neurons express NE, but there are also groups of neurons that co-express neuropeptides such as Galanin (Gal) or Neuropeptide Y (NPY) [18]. These different types of cells also show a bias in distribution: most multipolar neurons are found ventrally in the LC and most fusiform neurons dorsally, while Gal^+ neurons are located mostly in the dorsal and central LC and NPY^+ neurons only dorsally. Further topographical distinctions between LC neurons are also present on anatomical level: some cells in the LC are organized based on their efferent projections along the ventral-dorsal axis or the anterior-posterior axis. On the ventral-dorsal axis, neurons projecting to the forebrain are located more dorsally while neurons projecting to the cerebellum and spinal cord are located more ventrally. And on the anterior-posterior axis, neurons projecting to the thalamus are located more posteriorly, those projecting to the hypothalamus more anteriorly and neurons projecting to the cortex and amygdala are found all throughout the LC [19].

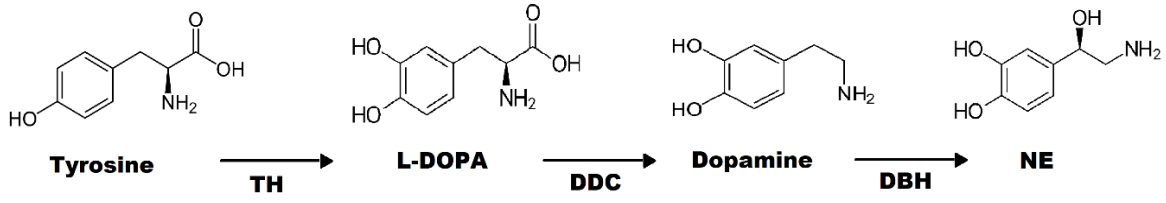

Fig. 3 Synthesis of norepinephrine from tyrosine (TH: tyrosine hydroxylase, DDC: DOPA decarboxylase, DBH: dopamine β-hydroxylase).

1.3.2 Receptors

Noradrenergic signaling in the brain is mediated through adrenergic receptors (AR). These are G protein-coupled receptors (GPCR) which can be divided in 2 classes: α ARs and β ARs. The α AR family knows 2 subfamilies: α1 AR, Gq-coupled receptors that signal via phospholipase C, and α2 AR, Gi-coupled receptors that inactivate adenyl cyclase. β ARs are coupled primarily to Gs and signal through the adenyl cyclase/cAMP pathway, but some subtypes also couple to Gi [20]. The α1- and β-receptors exist mostly postsynaptic, while the α2-receptors are found both post- and presynaptically **(Fig. 4)**. Binding of NE to these receptors can modulate excitability of target cells in complex ways, depending on distribution of receptor types and concentration of NE [16].

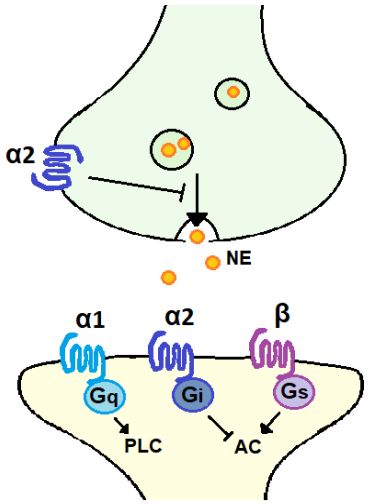

Fig. 4 Schematic drawing of the distribution of α and β adrenergic receptors (PLC: phospholipase C, AC: adenyl cyclase).

1.3.3 Activity/physiology

Neurons in the LC display synchronous discharge patterns and two distinct modes of firing: tonic and phasic. Tonic activity is present during waking and non-REM sleep, in which LC neurons produce slow, spontaneous discharges. The tonic discharge rate is state-dependent with the lowest rates during NREM sleep (<1Hz) and the highest rates during active waking in periods of arousal (up to 15 Hz). This tonic discharge pattern can be interrupted by phasic activity in response to a salient sensory stimulus. Phasic discharges are characterized by a burst of action potentials followed by a period of decreased firing [21, 22].

1.3.4 Functions

The LC-NE system modulates certain behaviors such as waking, as is evident from the neuronal activity patterns mentioned above. But the LC plays a role in many other functions such as attention, memory, synaptic plasticity and network resetting. Although the LC-NE system has varied modulatory actions on many cognitive functions, it is possible to assign an overarching function to it: the facilitation of responding to salient, significant stimuli in the environment. This is achieved first of all by acting on waking, which is necessary for the reception of sensory information. Then, in this state, the LC-NE system modulates multiple cortical and subcortical networks involved in cognitive functions to enhance the response to salient sensory stimuli and to suppress the response to irrelevant stimuli. This increase in signal to noise ratio of relevant sensory information allows for a shift in attention to ensure optimal behavior. Whether or not a stimulus is salient depends on the situation and the stimulus may be appetitive or aversive [16, 23].

1.4 Role of LC in VNS

The implication that the LC is involved in the anticonvulsive effects of VNS is supported by several studies. In 1998, Krahl et al. showed that in rats with chronic or acute lesions to LC, the VNS-induced seizure suppression was partially lost [24]. Additionally, it has been shown that VNS leads to activation of the LC and consequential release of NE, as increased firing of LC neurons and increased concentrations of extracellular NE in the cortex and hippocampus were measured during application of VNS [25, 26]. It is important to note that the LC cannot be solely responsible for the anticonvulsive effects seen in VNS treatment, as inactivation of the LC did not lead to complete loss of these effects. But these studies do prove that the LC plays an important role in VNS treatment. The antiepileptic effects of NE from the LC have also been studied unrelated to VNS, some even before VNS was used as treatment for epilepsy [27]. In various experimental models, it has been shown that NE exerts anticonvulsive effects while NE depletion leads to proconvulsive effects [28]. This was first clearly demonstrated in amygdala kindling in rats [29]. Kindling is a technique where epilepsy is induced by repeatedly

stimulating a brain structure, in this case the amygdala. When this was performed after NE depletion, the speed of the kindling process was accelerated while an increase in NE delayed the kindling. Likewise, in other epilepsy models with chemoconvulsants or electroconvulsive shock, NE depletion through damage to the LC increases seizure susceptibility while LC stimulation acts anticonvulsive. And loss of noradrenergic innervation is shown to convert sporadic seizures into status epilepticus, proving that NE is needed to limit the spread and duration of seizures.

While there is much evidence to assign certain antiepileptic effects of VNS to the LC, a recent finding calls for caution in interpreting some results of previous studies. Experiments in the 4Brain research lab showed that stimulating the vagus nerve in rats induces a decrease in brain and body temperature [30]. Application of a rapid cycle VNS paradigm (7s on/18s off) and of a standard cycle VNS paradigm (30s on/300s off) both lead to peripheral vasodilation and a decrease in brain and body temperature. As temperature is an important parameter in many physiological processes, this hypothermic effect could be a possible confounder in studies examining the effects of the LC in VNS. For instance, in a prior study at the 4Brain lab on VNS in rats a modulation in hippocampal excitability was witnessed [31]. The effects seen during VNS were initially hypothesized to be possibly caused by NE released from the LC. However, these changes on EEG could be solely due to a decrease in brain temperature as these changes were also described in hypothermic rats [32]. This then also prompted the follow-up experiments that led to the finding of the hypothermic effect of VNS.

Now, in order to investigate whether the modulation of hippocampal activity from the first study can be attributed to NE release, a new set of experiments where the LC is directly activated in rats is to be conducted. This way there is no influence of the VNS-induced hypothermia on the EEG, and thus only the effect of NE release can be studied. This direct activation can be achieved using chemogenetic or optogenetic methods.

1.5 Chemo- and optogenetics

Chemo- and optogenetics are two sets of experimental tools used in neuroscience that have a common concept. It involves transduction of specific neuron populations to express ‘activatable’ membrane proteins. Activation of these proteins then leads to either excitation or inhibition of the neurons. Selective expression of the membrane proteins in the desired cell types can be achieved through the use of transgenic animals or by delivering the required genes with a viral vector under control of a cell type-specific promotor.

The difference between the two techniques lies in the manner of activation. In case of chemogenetics, the membrane proteins are designer receptors that are sensitive to a specific, otherwise inert drug. Optogenetics on the other hand makes use of opsins that respond to light of a specific wavelength.

1.5.1 Chemogenetics

Several types of chemogenetic tools have been developed over the years [33]. One of the earliest chemogenetic receptors, dating back to the late 90’s, were engineered GPCRs called RASSLs (*receptors activated solely by synthetic ligands*) [34]. The initial RASSL was a κ-opioid receptor designed to be insensitive to native ligands but sensitive to the synthetic agonist spiradoline. Several other RASSLs were engineered later on, but due to problems with effects of used ligands on endogenous receptors and occasional constitutive activity these type of receptors were not well suited for in vivo studies and were of not much use in neurosciences.

However, a newer type of chemogenetic GPCRs, termed DREADDs (*designer receptors exclusively activated by designer drugs*), was developed in 2005 and since saw a wide application in neuroscience [35]. These DREADDs were created by engineering muscarinic receptors to be activated by the inert molecule clozapine N-oxide (CNO) using directed molecular evolution in yeasts. Depending on the type of muscarinic receptor, DREADDs can

couple to G_q G-proteins in which case activation leads to neuronal firing (hM1Dq, hM3Dq, hM5Dq) or to G_i G-proteins which leads to inhibition (hM2Di, hM4Di) **(Fig. 5)**.

Besides chemogenetic GPCRs, there also exist chemogenetic receptors that manipulate neuronal activity via ion channels. These include invertebrate and mammalian ligand gated ion channels (LGICs), but the most recent tools consist of engineered chimeric LGICs where pharmacologically selective ligand-binding domains (LBDs) are combined with functionally diverse ion pore domains (IPDs) [36]. A mutated LBD of the α7 nicotinic acetylcholine receptor (α7 nAChR) is used that is only sensitive for a synthetic molecule. These domains are called PSAMs (*pharmacologically selective actuator modules*) while the corresponding ligands are termed PSEMs (*pharmacologically selective effector molecules*). The type of IPD to which the PSAMs are fused then determines the ion conductance properties of the engineered LGIC and the effect on neuronal activity upon PSEM binding. For example, using the IPD of the serotonin receptor gives a cation conducting LGIC which depolarizes neurons. When the IPD of the glycine receptor is used, a LGIC with chloride conductance properties is created which inhibits neuronal excitability through hyperpolarization.

The use of chemogenetics has several advantages; administration of the ligand (CNO in case of DREADDs, PSEM in case of engineered LGICs) can be done non-invasively and requires no specialized equipment. The main disadvantage of chemogenetic tools is the lack of precise temporal control. For this, an optogenetic approach is more suited.

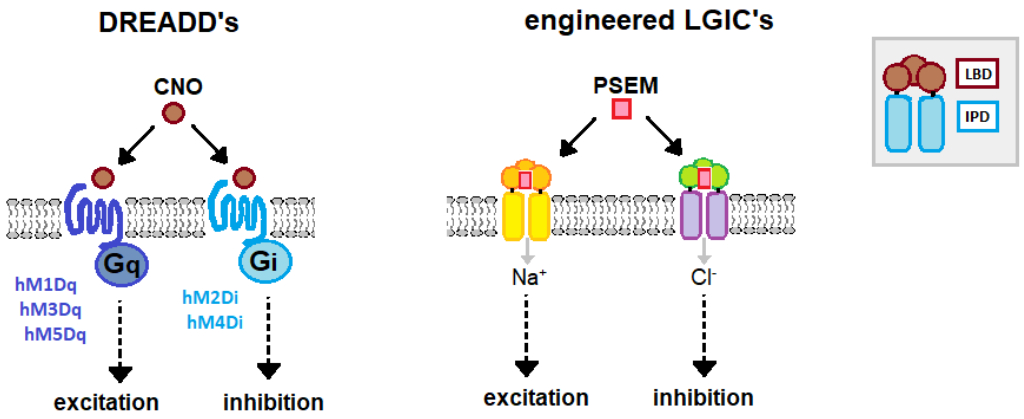

Fig. 5 Two major groups of chemogenetic receptors: DREADDs (*designer receptors exclusively activated by designer drugs*) are chemogenetic GPCRs activated by clozapine N-oxide (CNO) and signal though G-protein pathways, engineered LGICs (*ligand gated ion channels*) exist of a ligand binding domain (LBD) that can be activated by a PSEM (*pharmacologically selective effector molecule*) and an ion pore domain (IPD).

1.5.2 Optogenetics

Photoactivation of optogenetic constructs is achieved by the use of opsins. These are light-responsive, seven-transmembrane proteins of which two superfamilies exist: microbial opsins (type I) and animal opsins (type II) **(Fig. 6)** [37]. Opsins in both families require retinal, a vitamin A-derived cofactor, to function and opsins to which retinal is bound are referred to as rhodopsins. This retinal is the light-sensitive element and isomerizes upon absorption of photons, leading to structural changes and activation of the opsin proteins. Type I opsins are photo-sensitive ion channels while type II are GPCRs. This enables the choice in optogenetic tools between the use of ion channels or GPCRs, just as is the case with chemogenetics.

The first optogenetic tool to be used in neuroscience in 2005 was a type I opsin: the protein Channelrhodopsin-2 (ChR2) from the green alga *Chlamydomonas reinhardtii* [38]. This is a cation channel sensitive to blue light and was introduced in hippocampal neurons in which

photoactivation led to depolarization and millisecond-timescale control of spiking [39]. Since then, ChR2 has been improved on by conducting various modifications, for example to increase expression in mammalian cells. By now many more microbial opsins have been discovered, optimized and modified for use as optogenetic tools, such as Channelrhodopsin-1 (ChR1) and halorhodopsin. This has created an expansive toolbox of optogenetic ion channels with different properties: the wavelength of light needed for activation, ion conductance regulation properties and kinetics of the channels. The main opsin used in optogenetics for neuronal inhibition is an ion pump derived from the species *Natronomonas pharaonis* ; an enhanced halorhodopsin (eNpHR) [40]. Activation by yellow light leads to hyperpolarization in neurons by this chloride pump.

While type I opsins have seen the most use in optogenetics for their control over the membrane potential in neurons, mammalian type II opsins have also been developed as optogenetic tools for control over GPCR signaling pathways. These type of optogenetic proteins are known as optoXRs [41]. Since these proteins modulate biochemical signaling pathways, this type of optogenetics has a much broader use and can be applied in more, non-excitable cell types outside the field of neuroscience.

Activation of opsins in *in vivo* optogenetic experiment is mostly done using lasers. Delivery of laser light for stimulation of transduced tissue is done via optical fibers coupled to a laser system with cables. The fibers can be acutely implanted in the brain through cannulas or optical fibers can be permanently implanted. In both cases, this does make optogenetics a more invasive approach compared to chemogenetics.

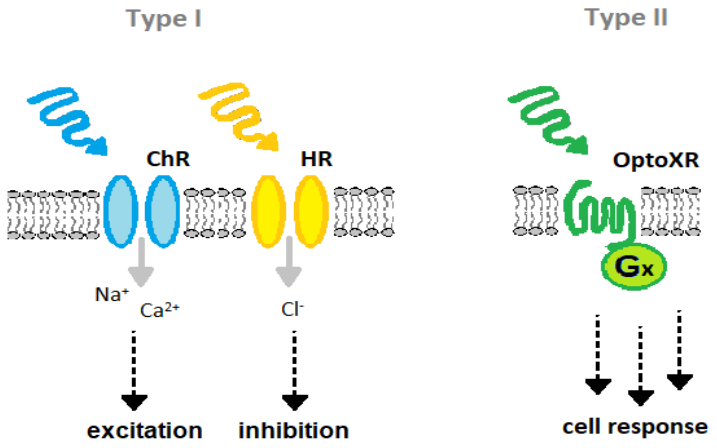

Fig. 6 The two types of opsins used in optogenetics. Type I opsins are photo-sensitive ion channels, including channelrhodopsins (ChR) and halorhodopsins (HR). ChRs are activated by blue light and conduct cations, HRs are chloride pumps activated by yellow light. OptoXRs are type II opsins that are activated by green light and signal through G-protein pathways.

1.6 Research objective

As mentioned previously, it is evident from literature that the LC-NE system has a role in the anticonvulsive effects of VNS: during stimulation the LC is activated to release NE and damage to the LC leads to partial loss of anticonvulsive effects [24-26]. But further research is needed to elucidate how exactly the LC-NE system helps suppress seizures. Some of the current research that is being conducted focuses on excitability.

As neuronal excitability is an important aspect in epilepsy, a prior study examined the effects of VNS on excitability in the hippocampus of rats [31]. This study revealed a complex change in hippocampal excitability during VNS application by looking at dentate gyrus evoked potentials (EPs) and the hippocampal electroencephalogram (EEG). Electrical stimulation in the perforant path leads to excitatory synaptic transmission at the dentate gyrus, shown by a

field excitatory post-synaptic potential (fEPSP) on the EEG. This excitatory synaptic transmission is followed by generation of action potentials in the dentate granule cells, leading to a population spike superimposed on the fEPSP. VNS application resulted in a decreased fEPSP slope and increased population spike latency and amplitude in the dentate field EP recordings **(Fig. 7)**. On the hippocampal EEG, slowing of the theta rhythm and reduced power of the theta peak and gamma band were observed. It was hypothesized that increased NE signaling in the hippocampus could explain these changes. However, a follow-up study revealed that VNS induces hypothermia and this could be the cause of the observed changes in excitability [30].

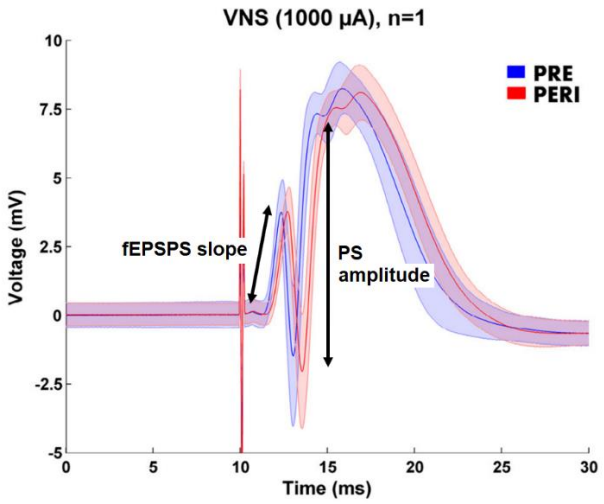

Fig. 7 Effect of VNS on dentate field evoked potentials. The slope of the field excitatory post-synaptic potential (fEPSP) decreased while the amplitude and latency of the population spike (PS) increased during VNS application (PERI, red) compared to the period before VNS (PRE, blue).
Figure adapted from Larsen LE (2016) [31]

Now, the objective of this project is to examine whether the LC is involved in the modulation of hippocampal excitability. Thanks to the available chemo- and optogenetic tools, the effects of NE can be examined through direct LC activation. This way, any side-effects that could occur when the LC is activated indirectly via VNS, such as hypothermia, can be avoided. Modulation of the noradrenergic neurons of the LC is obtained by stereotaxic injection of a viral vector carrying a excitatory chemo- or optogenetic construct. Preliminary experiments using chemogenetic approaches (DREADD and PSAM constructs) yielded unsatisfying results regarding the expression of the chemogenetic proteins on the targeted noradrenergic neurons [42]. For this reason, it was decided to switch to optogenetic manipulation and to proceed using a viral vector containing the ChR2 opsin. In the first phase of this project, expression of the opsin in the LC will be validated and optimized. If this results in acceptable expression levels, the second phase of the experiments can be executed in which optogenetic stimulation of the LC will be conducted in conjunction with dentate field EPs and hippocampal EEG recordings. Simultaneously, extracellular NE concentrations can be measured in the hippocampus through microdialysis. This is an in vivo sampling technique that can be used to measure analyte concentrations in extracellular fluids. By inserting a microdialysis probe through a guide cannula implanted into the hippocampus, hippocampal NE concentrations can be measured to verify if optogenetic LC stimulation leads to the expected NE release and possible correlations between extracellular NE concentration and hippocampal excitability can be studied.

2. Materials & Methods

2.1 Animals

In the main experiments, male adult Wistar Hannover (WH) rats (350-450g at time of viral vector injection, Janvier Laboratories) were used. Additionally, 2 male adult Fischer rats (350g at time of viral vector injection, Charles River Laboratories) were also used. The animals were housed in individual cages under environmentally controlled conditions at a 12h/12h light/dark cycle. Food and water were *ad libitum* available. Animals were handled for at least 1 week before any procedure. All procedures were conducted in accordance with the Animal Experimental Committee of Ghent University Hospital (ECD 16/31) and in accordance with the European directive 2010/63/EU.

2.2 Viral vector

Transduction of LC neurons was done using a canine adenovirus type 2 (CAV2) vector containing the sequence for ChR2 coupled to a mCherry tag preceded by the PRSx8 promoter (CAV2-PRSx8-ChR2-mCherry), obtained from the group of prof. Pickering [43]. CAV2 vectors preferentially transduce neurons and distribute via axonal transport [44]. The PRSx8 promoter is a synthetic promoter specific for noradrenergic neurons containing several copies of a *cis*-regulatory element (PRS2) of the DBH promoter [45]. Finally, mCherry is a small monomeric red fluorescent protein which sequence is tagged on to the sequence coding for ChR2. Cells that are successfully transduced by this viral vector express the ChR2 together with mCherry for visualization.

2.3 Construction of optical fibers

Implantable optical fibers were manually constructed to obtain fibers with a desired length of ~7mm to insert into LC at a ventral depth of ~5.5mm **(Fig. 8)**.

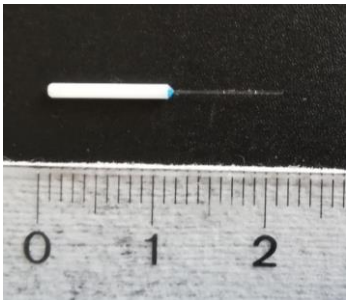

Fig. 8 Example of a manually constructed optical fiber.

First, insulation of the optical fiber (Ø200 µm core multimode optical fiber, low OH, 0.39 NA, Thorlabs, FT200EMT) from the fiber spool was stripped off using a fiber stripper tool (typical cladding/coating: 230 µm / 500 µm, Thorlabs, T12S21). Pieces of fiber with a length of ~20mm were detached from the spool by scoring (making a small cut) the fiber with a diamond knife and pulling at the fiber until it snapped. This method makes it possible to acquire pieces of fiber with a clean, straight end without damaging the core of the fiber. The scored end of each fiber was checked under a microscope to determine if there was no damage to the fiber core. Next, fibers were inserted into ferrules with the scored, straight end pointed at the flat side of the ferrule and leaving ~7mm of the fiber exposed (this side was inserted into the brain). A drop of epoxy adhesive (Hysol TRA-BOND F112, Henkel-adhesives) was added to the flat end of the ferrules to glue the fibers and the ferrules together. The glued fibers were left to dry for 24h. Finally, the remaining exposed fiber at the convex side of the ferrules was removed by scoring the fiber and tapping it off. The fibers were then inserted into a polishing disc and the convex end of the ferrules was polished on four grades of polishing paper (30, 6, 3, 1 µm).

After construction of the optical fibers, each fiber was tested to determine the percentage of light attenuation when coupled to the laser (473nm Blue DPSS Laser, SLOC Lasers) via a patch cable. Only optical fibers with an attenuation of >70% were accepted and used for implantation.

2.4 Surgical procedures

2.4.1 Stereotaxic injections

Injections of the viral vector were made into the LC using stereotaxic coordinates. Before surgery, the surgery table and equipment were cleaned and disinfected using 70% ethanol. The surgical instruments were sterilized using an autoclave. The Hamilton syringe (Model 7001, 1 µl, blunt tip) was rinsed with Hamilton cleaning solution (10x), distilled water (10x) and ethanol (1x). Animals were anesthetized in a transparent box with 5% isoflurane (IsoFlo®, Zoetis, Belgium) and 8l/min medical oxygen until loss of paw withdrawal reflex. After induction of anesthesia, animals were moved into the stereotaxic frame and anesthesia was maintained with 1-2% isoflurane and 1l/min oxygen. A heating pad was used to keep the animals' body temperature around 37°C. Xylocaine (Xylocaine jelly 2%, AstraZeneca, Belgium), a local analgesic, was applied to the ear bars which were used to fixate the head of the animal. Duratears (Alcon NV, Belgium) were applied on the eyes to protect them from dehydration. Surgery started with shaving of the head and administering a subcutaneous injection of Xylocaine mixed with adrenaline (1mg/kg, AstraZeneca, Belgium) for extra local anesthesia and vasoconstriction of the blood vessels. A midline incision was made in the scalp to expose the skull. The surface of the skull was cleaned with saline and the coordinates of Bregma (intersection of the coronal and the sagittal suture) and Lambda (intersection of the lambdoid and the coronal suture) were measured **(Fig. 9)**. These coordinates were used to calculate and mark the positions for injection. Next, a craniotomy was made around the site marked for injection using a small drill. Animals were then repositioned in the frame to position Bregma -2mm relative to Lambda to achieve a ±15° rostral angulation. The Hamilton syringe was mounted on the frame and injections of the CAV2-PRSx8-ChR2-mCherry vector (titre 1.3x10E12 TU/ml, 5 times diluted in sterile PBS) were made at a flowrate of 150 nl/min with a 5 min pause between injections. Injections in the LC were performed unilaterally or bilaterally. Per injection site, 3 injections of 300 nl were administered along the dorsoventral axis (coordinates: AP -3.9mm, ML ±1.15mm relative to Lambda, DV -5.8/5.5/5.3mm relative to dura). The syringe was slowly pulled out 5 minutes after the last injection to prevent outflow of the vector. Afterwards, the skin was closed with non-degradable stiches, Xylocaine gel was applied and a subcutaneous injection of meloxicam (nonsteroidal anti-inflammatory drug,1mg/kg, Metacam®, Boehringer Ingelheim, Germany) was administered for pain relief.

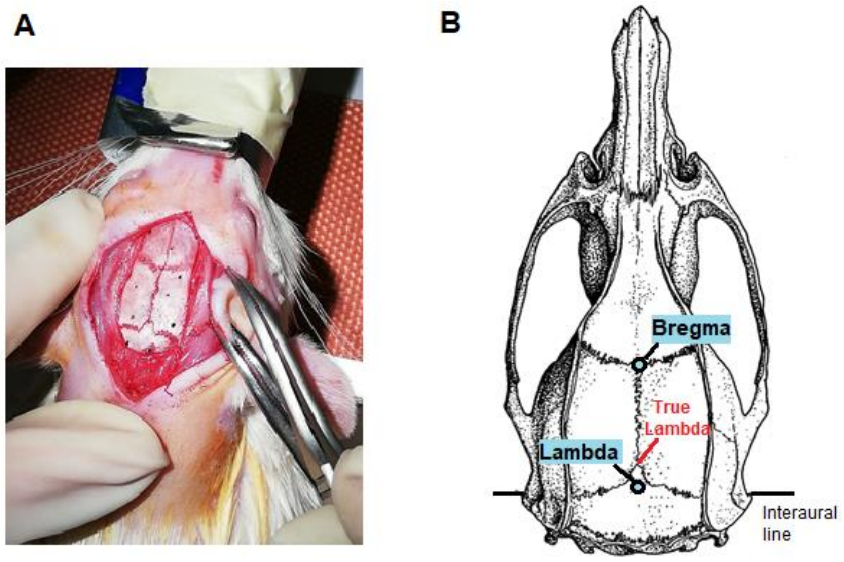

Fig. 9 (A) Exposing the skull reveals the sutures used to determine the reference points needed for stereotaxic injections. **(B)** Bregma is the point of intersection of the sagittal suture with the coronal suture. While Lambda is defined as the midpoint of the curve of best fit along the lambdoid suture, the true Lambda (the point of intersection of the sagittal and lambdoid sutures) is usually taken as reference point during surgery.

2.4.2 Implantation of optical fibers

Surgery on animals that were implanted with optical fibers required some extra steps. After exposing and cleaning the skull with saline, the surface of the skull was roughened to ensure better attachment of dental cement. The skull was cleaned using acetone and scratches were made on the surface using a scalpel. Next, coordinates were marked and craniotomies were made as described in detail above. Additional holes were drilled for the placement of anchor screws, used to stabilize the optical fiber, which were afterwards glued in place with dental adhesive (Super-Bond C&B, Sun Medical Co., Japan). After the injections, optical fibers were slowly lowered into the LC on the same coordinates (AP -3.9mm, ML -1.15mm relative to Lambda, DV -5.5/5.3mm relative to dura). Once in place, the fibers were fixed to the skull and anchor screws with a base layer of UV-cement and further fixated using dental acrylic cement.

2.5 Histology

2.5.1 Transcardial perfusion

Two weeks after viral vector injection, rats were sacrificed to examine transgene expression. The animals were anesthetized using 5% isoflurane and euthanized with an intraperitoneal overdose of pentobarbital (Dolethal, 0.1ml/100g, Vétoquinol, Belgium). The thoracic cavity was opened and heparin (Heparine® LEO, Leo Pharma, Belgium) was injected into the heart to prevent blood clotting. A blunt needle was inserted in the aorta via the apex of the heart. A small incision in the right atrium was made followed by transcardial perfusion with phosphate buffered saline (PBS, 10 minutes) and paraformaldehyde solution (4% in PBS, 10 minutes) for fixation of the brain.

2.5.2 Cryosectioning

The brains were isolated from the skull and consecutively put in 10%, 20% and 30% sucrose solution for cryoprotection and snap frozen in isopentane (2-methylbutane, Sigma-Aldrich) cooled with liquid nitrogen. They were then stored in a -80°C freezer until sectioning. The brains were sectioned into slices of 40 µm on a cryostat (Leica CM 3050 S Cryostat). Slices at the level of the brainstem containing the LC were collected from all subjects. Additionally, slices containing the hippocampus were collected in a subset of animals.

2.5.3 Immunohistochemistry (IHC)

Brain slices were rinsed in distilled water (2x 5 min), followed by incubation in H_2O_2 (30 min in 0.5%, 60 min in 1%) to block endogenous peroxidase activity. Then, slices were rinsed in PBS (2x 5 min) and put in blocking buffer (BB; 0.2% Triton X-100 / 0.4% Fish Skin Gelatin / PBS) for 45 minutes to reduce background staining. Primary antibodies were added to the brain slices dissolved in BB, which were left to incubate overnight. To visualize noradrenergic neurons on LC slices, mouse anti-TH antibodies were used (1:1000, clone LNC1, Sigma-Aldrich). On the hippocampal slices, mouse anti-DBH antibodies (1:1000, clone 4F10.2, Sigma-Aldrich) were used to visualize noradrenergic axons. To visualize transgene expression, rabbit anti-RFP (red fluorescent protein) antibodies were used (1:1000, Rockland, Tebu-Bio) against the mCherry tag. For positive controls, mouse anti-NeuN antibodies (1:1000, clone A60, Millipore/Chemicon) and rabbit anti-Glial Fibrillary Acidic Protein antibodies (1:1000, Sigma-Aldrich) were used. For negative controls, BB without antibodies was added. The following day, Alexa Fluor secondary antibodies dissolved in BB (1:1000, Alexa F goat anti-mouse 488 nm, Ab150113, and Alexa F goat anti-rabbit 594 nm, Ab150088, Abcam) were added after washing with BB (2x 10 min). After incubating for 1 hour, the slices were washed with PBS (2x 5 min). Nuclear staining was performed with DAPI-solution (4',6-diamidino-2-phenylindole). The brain slices were washed again in PBS (2 x 5 min) and mounted on glass microscope slides with Vectashield Mounting Medium Fluorescence, coverslips and nail polish.

2.6 Fluorescence microscopy

Images of the stained slices for analysis of opsin expression were acquired with AxioVision Microscope Software (6D acquisition) connected to a Carl Zeiss fluorescence microscope. For

manual cell counting, confocal images with an increased optical resolution and contrast were made with an Olympus confocal microscope IX81 and Fluoview 1000 Software. The contrast/brightness of all images was optimized using Fiji-ImageJ software.

2.7 Analysis of expression levels

The levels of opsin expression in the targeted noradrenergic neurons were initially qualitatively assessed on the images of the immunofluorescence stainings. Cells of the LC were visualized by Alexa Fluor 488 nm antibodies and displayed green fluorescence while red fluorescent Alexa Fluor 594 nm antibodies indicated the presence of ChR2. Thus, double positive cells (red and green fluorescent) were LC neurons that had been successfully transduced and expressed the opsin. Cells that only displayed a red fluorescent signal were a sign of non-specific opsin expression not restricted to LC neurons.

For quantification of expression levels, two methods were applied. First, images captured on the Zeiss fluorescence microscope were processed using ImageJ software to calculate the ratio of red versus green fluorescence. For every image, the red and green color channels were converted to grayscale (8 bit) images. On these 8 bit images the *Threshold* function in ImageJ was used to separate the background fluorescence signal from the fluorescence signal indicating LC neurons on the green channel or mCherry on the red channel. This way, all pixels in the image were given a binary value: pixels with an intensity above the threshold were converted to white, pixels below the threshold were converted to black. The *Histogram* function was then used to count the number of white pixels as measurement for the amount of (non-background) fluorescence. Expression levels were finally calculated as the ratio of red fluorescence over green fluorescence by dividing the number of white pixels on the red channel by the number of white pixels on the green channel and expressed as percentages (for protocol, see **Addendum 1**). Per animal, the average of the resulting expression levels was calculated twice. Once based on all the images acquired from the stained slices and once based on a selection of images with the best quality (images where the LC is clearly visible and where no artefacts are present, see **Addendum 3**). These results are reported as the average ± standard deviation.

The second method of quantifying expression consisted of a manual cell count on images captured on a confocal microscope. Per animal, one confocal image of the LC was obtained on which cells were manually counted using ImageJ. This was done by first counting the amount of clearly distinguishable noradrenergic neurons with a visible nucleus: markers were added to TH^+ cell bodies (green) containing a DAPI-stained nucleus (blue) on a merged image of the green and blue channels. Then these markers were transferred to a merged image of the green and red channels. This way, the marked cells that were double positive (TH^+ and $mCherry^+$) could be counted. Expression levels were then calculated as the number of double positive cells over the total number of marked cells and expressed as percentages (for protocol, see **Addendum 2**). These expression levels could then be compared to the levels acquired with the first method on the corresponding epifluorescence microscopy images.

3. Results

3.1 Phase 1: Validation/optimization of opsin expression

3.1.1 Pilot experiment

As a pilot trial, 3 animals (WH rats) were unilaterally injected with the CAV2-PRSx8-ChR2-mCherry vector in the LC. Evaluation of the IHC stainings showed successful expression of opsins in the targeted LC in all 3 animals; there was full overlap of red fluorescent mCherry signal on the green fluorescent LC neurons and red/green ratio measurements all exceeded 100% **(Fig. 10, Table 1)**.

After the positive results of this small pilot trial, the main experiments could start with a larger number of animals.

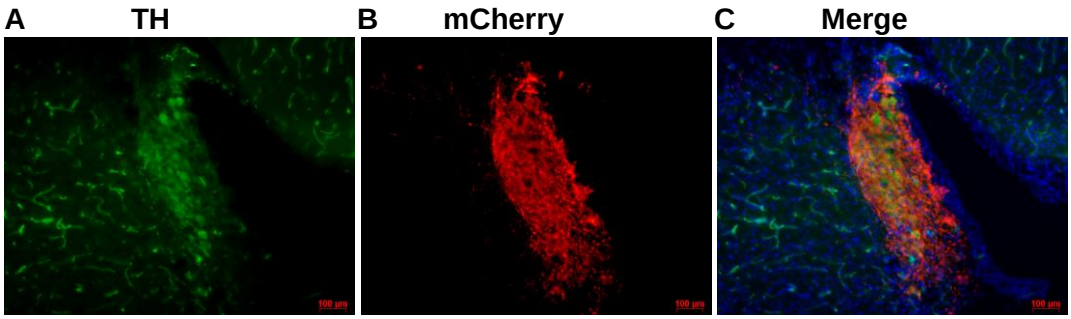

Fig. 10 Example of an immunohistochemical staining from the pilot trial, showing full overlap between the green fluorescent TH^+ neurons of the LC **(A)** and the red fluorescent opsin expression **(B)** on the merged image **(C)**.

Table 1: *Immunohistochemical and quantitative results of the pilot experiment.*

Animal ID		
CAVLC1	**CAVLC2**	**CAVLC3**
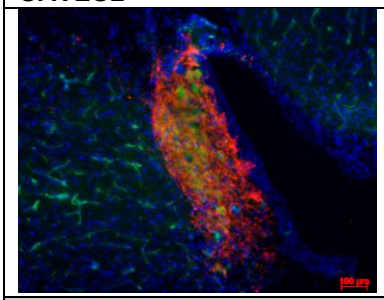	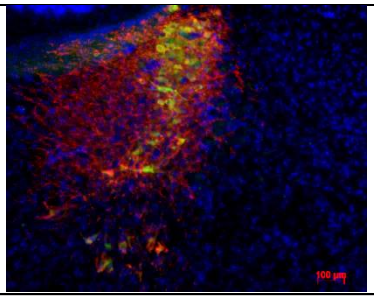	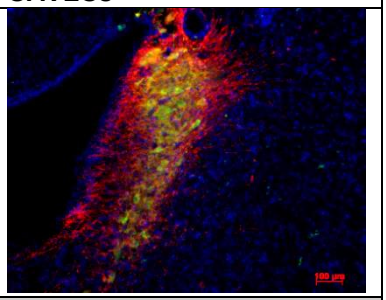
Red/green fluorescence ratio (average over *n* images)		
863,13% (n=1)	**576,42%** (n=1)	**344,06%** (n=2)

3.1.2 Unilateral injections and implantations

A first set of animals (WH rats, n=8) received a unilateral injection of the CAV2-PRSx8-ChR2-mCherry vector of which half was also implanted with an optical fiber. Two animals passed away during surgery after the craniotomy. Of the 6 remaining animals that successfully underwent the operation, 3 received solely an injection of the vector and 3 received an injection plus implantation of an optical fiber. Qualitative assessment of opsin expression on the IHC stainings showed a low rate of success: 2 out of 6 animals displayed good expression levels. No difference could be noted between the group that was solely injected and the group that was also implanted with a fiber, as both groups contained 1 animal with successful transduction of the LC and 2 animals with no or very weak opsin expression levels **(Table 2)**.

Table 2: *Overview of the immunohistochemical results of the group of animals that was unilaterally injected and the group that received a unilateral injection and fiber implantation.*

INJECTION		
Animal ID		
LSO1	LSO2	LSO3
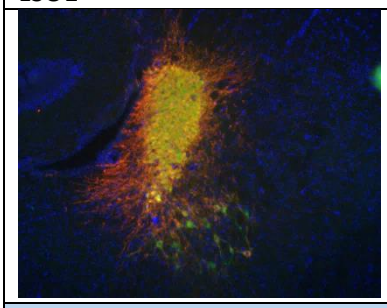	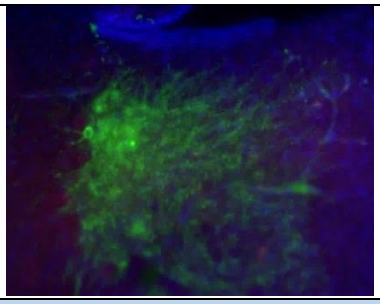	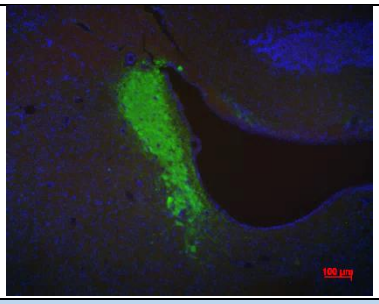
INJECTION + FIBER IMPLANTATION		
Animal ID		
LSO6	LSO7	LSO8
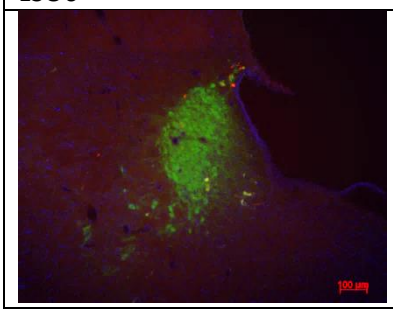	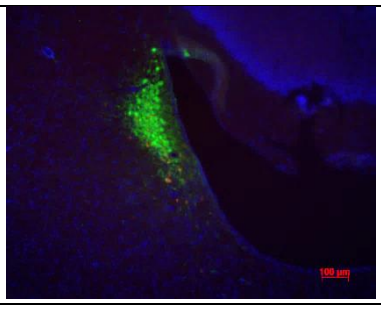	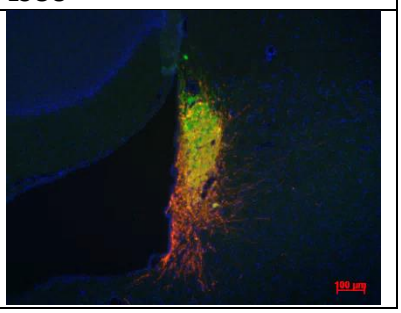

The first animal (ID: LSO1) possessed a successfully transduced LC. Expression of mCherry was ubiquitous in the targeted LC **(Fig. 11 A)**. This success was also confirmed by quantification of opsin expression: the average red/green fluorescence ratio over all images was 283,12% (± 147,47%, n=10) while the ratio based on high quality images was 162,99% (± 21,07%, n=3). Manual cell counting on the confocal image of one slice resulted in a more informative expression level of 90% (36/40 double positive neurons, **Fig. 11 C**) compared to the 165,35% red/green ratio of that slice.

On none of the slices of the second animal (ID: LSO2) and the third animal (ID: LSO3) there was any sign of opsin expression **(Fig. 12)**. As there was no signal of mCherry, there was no need for quantification.

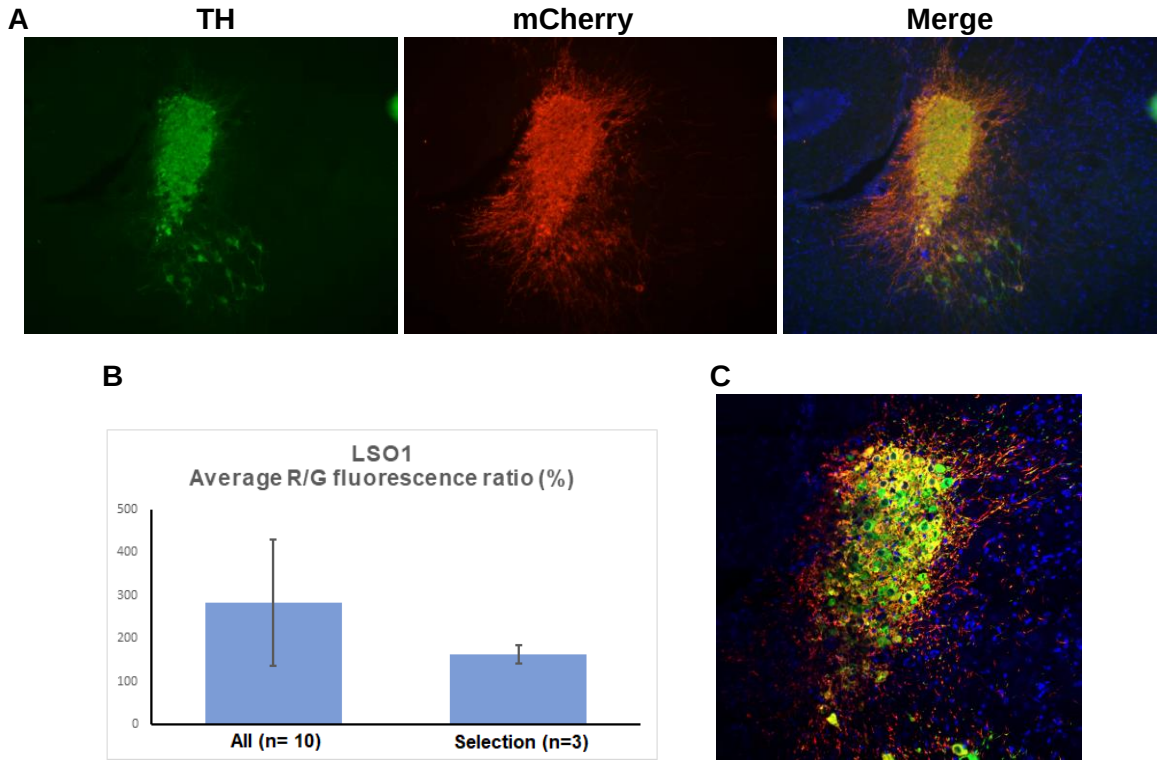

Fig. 11 Immunohistochemical results of LSO1. **(A)** Left: tyrosine hydroxylase (TH) staining of LC neurons. Middle: mCherry expression indicating extensive opsin expression in the LC. Right: merged image of the TH, mCherry and DAPI staining. **(B)** Graph of the ratios between red and green fluorescence, averaged over all immunofluorescence images (left bar) or over a selection of high quality images (right bar). **(C)** Image of the LC acquired on a confocal microscope used for manual cell counting.

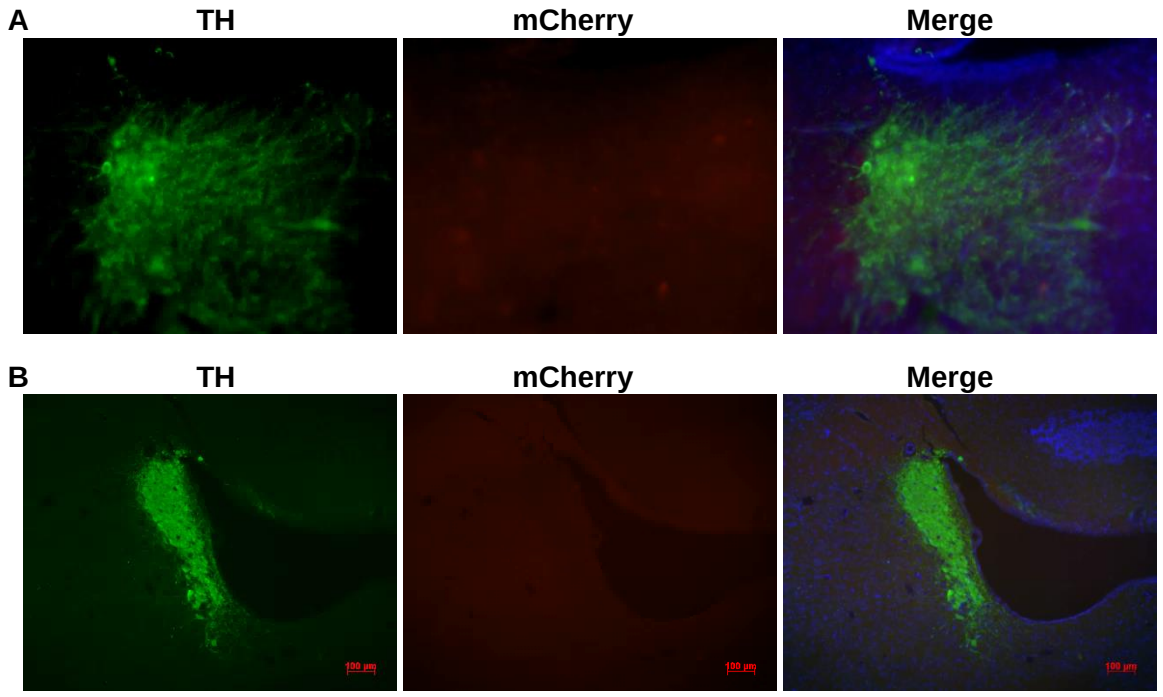

Fig. 12 Immunohistochemical results of LSO2 **(A)** and LSO3 **(B)**. Left: tyrosine hydroxylase (TH) staining of LC neurons. Middle: absence of mCherry expression indicating failure of transduction. Right: merged image of the TH, mCherry and DAPI staining.

Results of the fourth animal (ID: LSO6) were also negative. Transduction of the LC had failed. However, unlike in the previous two animals, there were some red spots visible on the immunofluorescence stainings indicating a very small amount of mCherry expression **(Fig. 13 A)**. The average red/green fluorescence ratio over all images was 10,61% (±9,68%, n=8) while the ratio based on high quality images was 3,45% (± 1,17%, n=2). The confocal image obtained for cell counting revealed that the red fluorescence was not present on any cell bodies, only on sections of axons and presumably some artefacts **(Fig. 13 C)**. So no counting was necessary on this slice, the expression level was 0% as there were no mCherry+ neurons visible, while the corresponding red/green ratio was 4,62% in that LC.

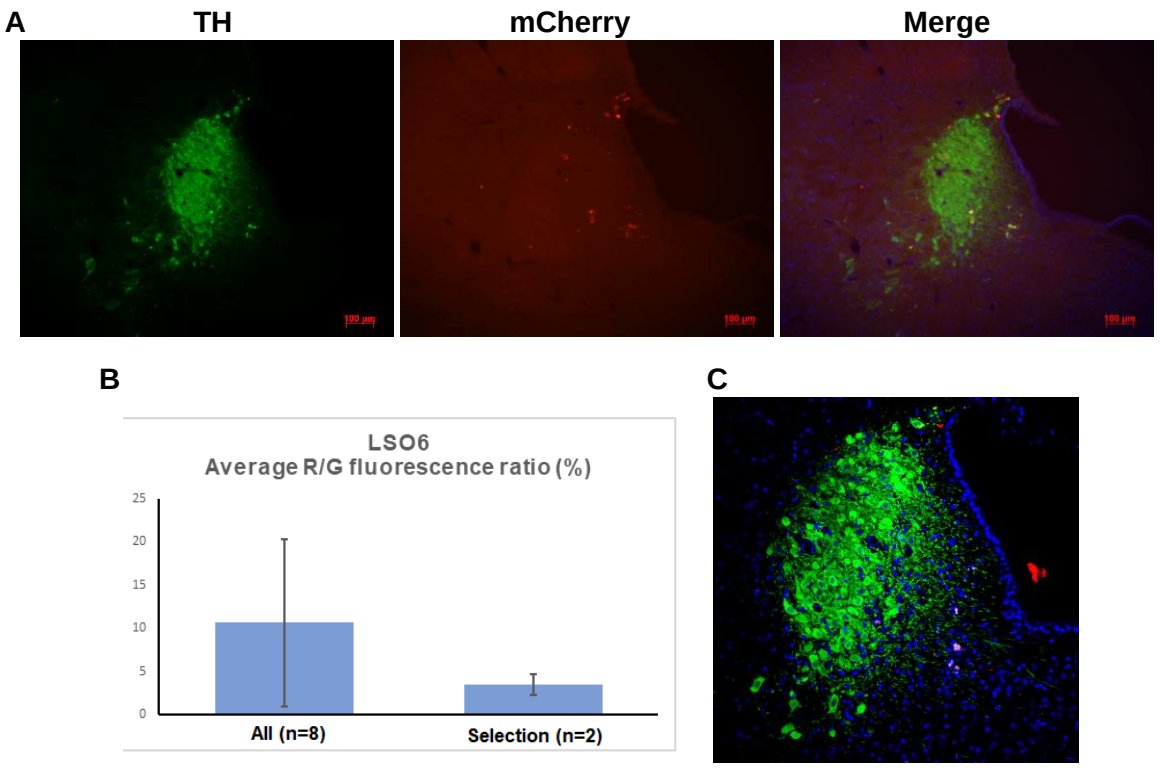

Fig. 13 Immunohistochemical results of LSO6. **(A)** Left: tyrosine hydroxylase (TH) staining of LC neurons. Middle: limited mCherry expression indicating small amounts of opsin expression. Right: merged image of the TH, mCherry and DAPI staining. **(B)** Graph of the ratios between red and green fluorescence, averaged over all immunofluorescence images (left bar) or over a selection of high quality images (right bar). **(C)** Image of the LC acquired on a confocal microscope used for manual cell counting.

On one of the slices in this animal the fiber tract was visible **(Fig. 14)**. This revealed substantive damage to the LC, indicating that the fiber was inserted too deep when implanted -5.5mm dorsoventrally from dura. Therefore, in following implantations the dorsoventral coordinates for insertion of the optical fiber were changed to -5.3mm relative to dura.

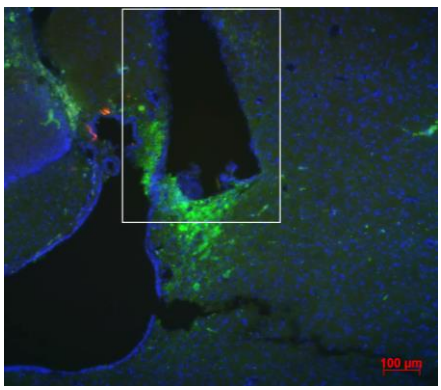

Fig. 14 Slice of LSO6 with a visible tract of the implanted optical fiber in the marked area.

The fifth animal (ID: LSO7) displayed similar weak opsin expression as the previous one, only very low amounts of mCherry were visible on the stainings **(Fig. 15 A)**. Quantification of expression levels gave the following results: an average red/green fluorescence ratio over all images of 8,74% (± 5,17%, n=6) and if based on high quality images of 9,12% (± 5,06%, n=3). And idem to the fourth animal, the expression level based on the confocal image was 0% while the red/green ratio was 13,43% since the low amount of red fluorescent signal originated from some axonal extensions **(Fig. 15 C)**.

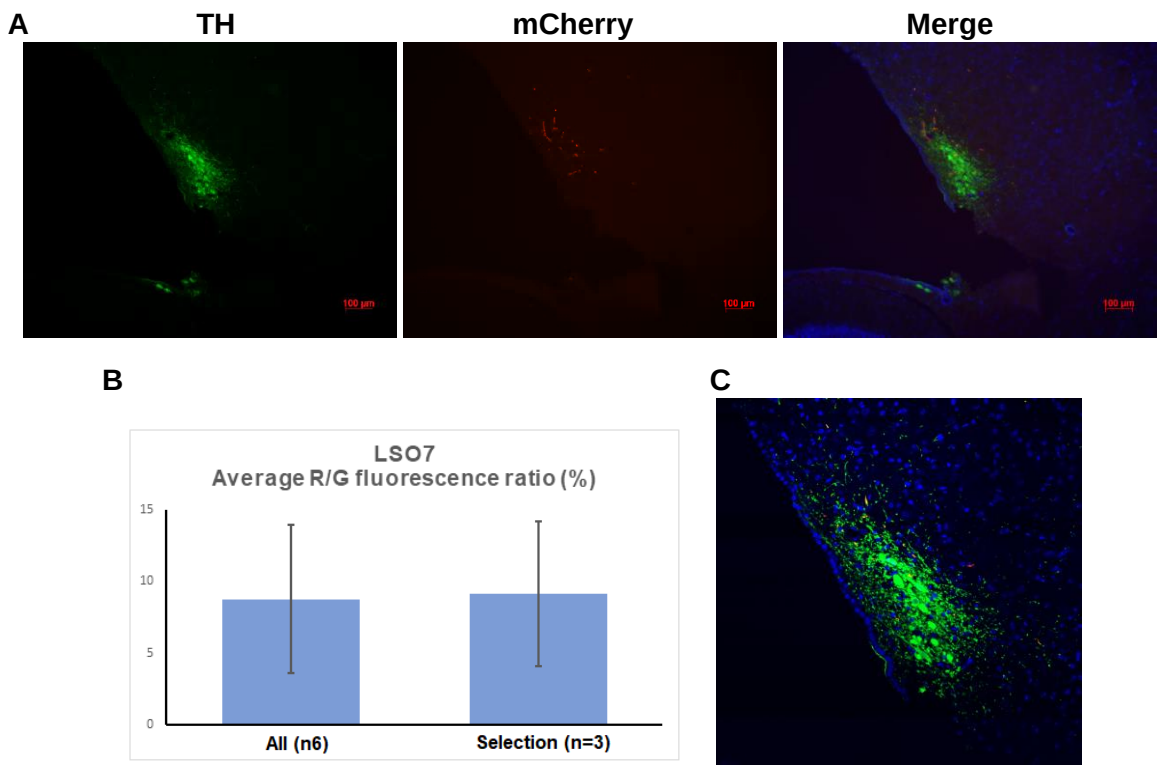

Fig. 15 Immunohistochemical results of LSO7. **(A)** Left: tyrosine hydroxylase (TH) staining of LC neurons. Middle: limited mCherry expression indicating small amounts of opsin expression. Right: merged image of the TH, mCherry and DAPI staining. **(B)** Graph of the ratios between red and green fluorescence, averaged over all immunofluorescence images (left bar) or over a selection of high quality images (right bar). **(C)** Image of the LC acquired on a confocal microscope used for manual cell counting.

The LC of the last animal (ID: LSO8) was successfully transduced. The images showed the mCherry signal covering most of the noradrenergic neurons **(Fig. 16 A)**. High expression levels were also obtained after measurement of the fluorescence: the average red/green fluorescence ratio over all images was 238,58% (± 83,83%, n=7) and the ratio based on high quality images was 147,01% (± 18,73%, n=2). Again, on the LC of one slice a more nuanced expression level of 66,67% (16/24 double positive neurons) was obtained after manual cell counting compared to the expression level of 165,74% based on the first quantification method **(Fig. 16 C)**. It must be noted however that this confocal image was of lower quality due to too high intensities used during capturing, making it more difficult to count.

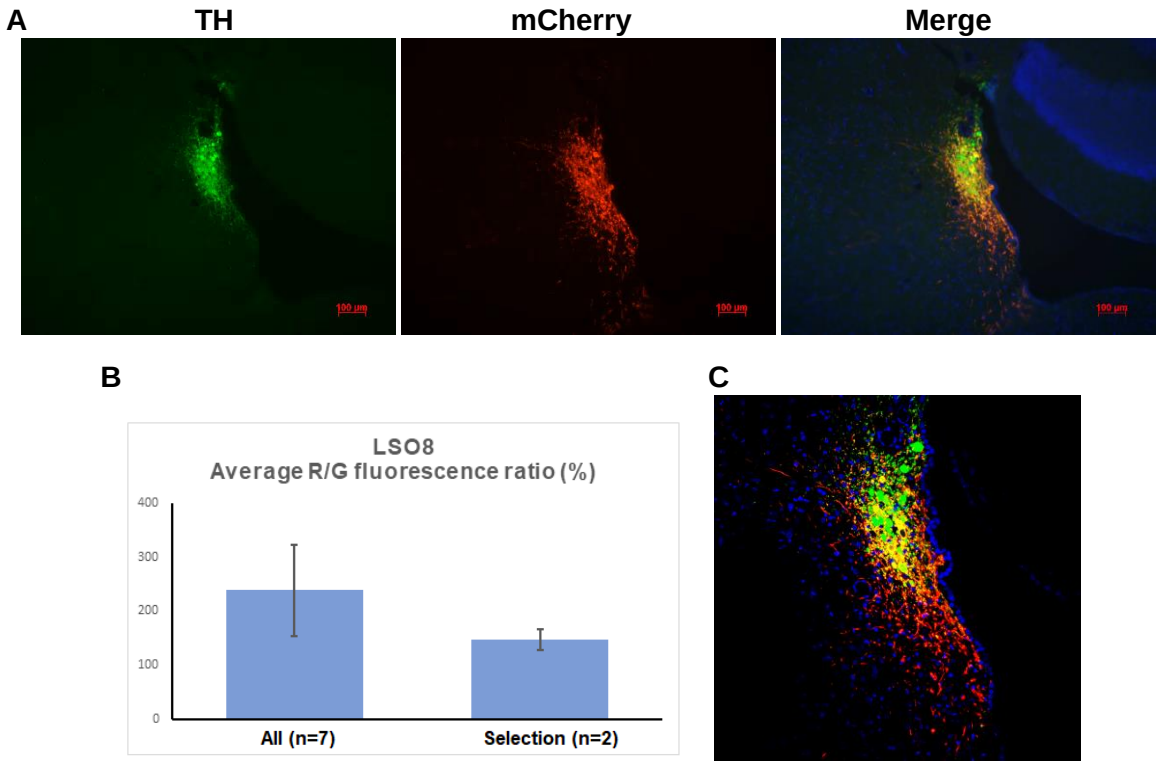

Fig. 16 Immunohistochemical results of LSO8. **(A)** Left: tyrosine hydroxylase (TH) staining of LC neurons. Middle: mCherry expression indicating extensive opsin expression in the LC. Right: merged image of the TH, mCherry and DAPI staining. **(B)** Graph of the ratios between red and green fluorescence, averaged over all immunofluorescence images (left bar) or over a selection of high quality images (right bar). **(C)** Image of the LC acquired on a confocal microscope used for manual cell counting.

3.1.3 Bilateral injections and implantations

Two Fischer rats that were ordered for a different research project but were no longer needed, were used for personal practice of the injection procedure and for testing the practicality of a bilateral implantation of optical fibers. These animals both received a bilateral injection of the CAV2-PRSx8-ChR2-mCherry vector in the LC together with a bilateral implantation of optical fibers. Unfortunately, due to a mistake during the fixation procedure, the brain tissue of these animals was not well preserved, leading to loss of some histological results. Only some IHC stainings of one of the animals could be qualitatively examined on images of lower quality, displaying successful transduction **(Fig. 17)**. Inspection of the bilateral fiber implantation after isolation of the brains was still possible however and showed uneven placement of the fibers in both animals.

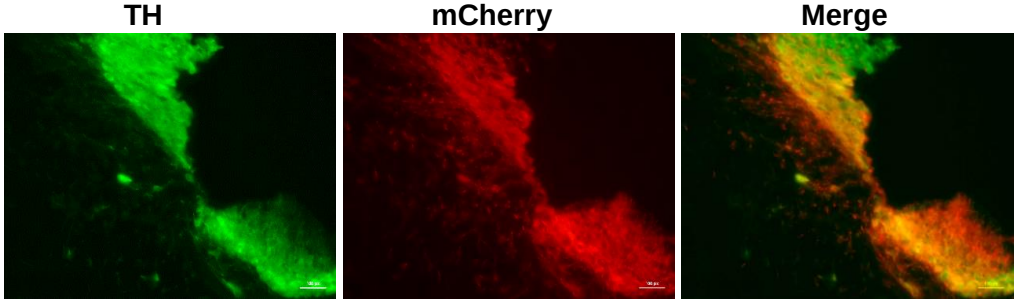

Fig. 17 Remaining immunohistochemical results of the injections in the Fischer rats. Left: tyrosine hydroxylase (TH) staining of LC neurons. Middle: mCherry expression indicating the expression of opsins in LC neurons. Right: merged image of the TH and mCherry staining.

3.1.4 Bilateral injections

Because of the unsatisfactory results in the first group of animals, a second set of WH rats (n=6) was bilaterally injected with the CAV2-PRSx8-ChR2-mCherry vector. One animal died during surgery. Brain tissue of the 5 remaining animals was collected, but in one animal fixation of the tissue had failed (presumably due to a problem during perfusion). This left the histological results of bilateral injections in 4 animals and thus 8 injection sites. An initial qualitative assessment showed varying results of expression levels per animal.

In the first animal (ID: JOEL1) both nuclei were successfully transduced. Both the left and right LC displayed a good amount of opsin expression on the IHC stainings, but the highest amount of expression was always present on the left side of each slice **(Fig. 18 A)**. This could also be observed in the results of the red/green fluorescence ratios. On the right, the average ratio over all images was 85,67% (± 32,14%, n=8) and the average of high quality images was 76,54% (± 17,66%, n=5). On the left the ratios were higher, with an overall average and an average after selection of 111,31% (± 19,98%, n=8) and 121,37% (± 12,74%, n=6) respectively. In this animal, a confocal image of the left LC was captured for manual cell counting **(Fig. 18 C)**. The resulting expression level was 89,47% (51/57 double positive neurons), which was slightly lower than the corresponding red/green ratio of 99,53%.

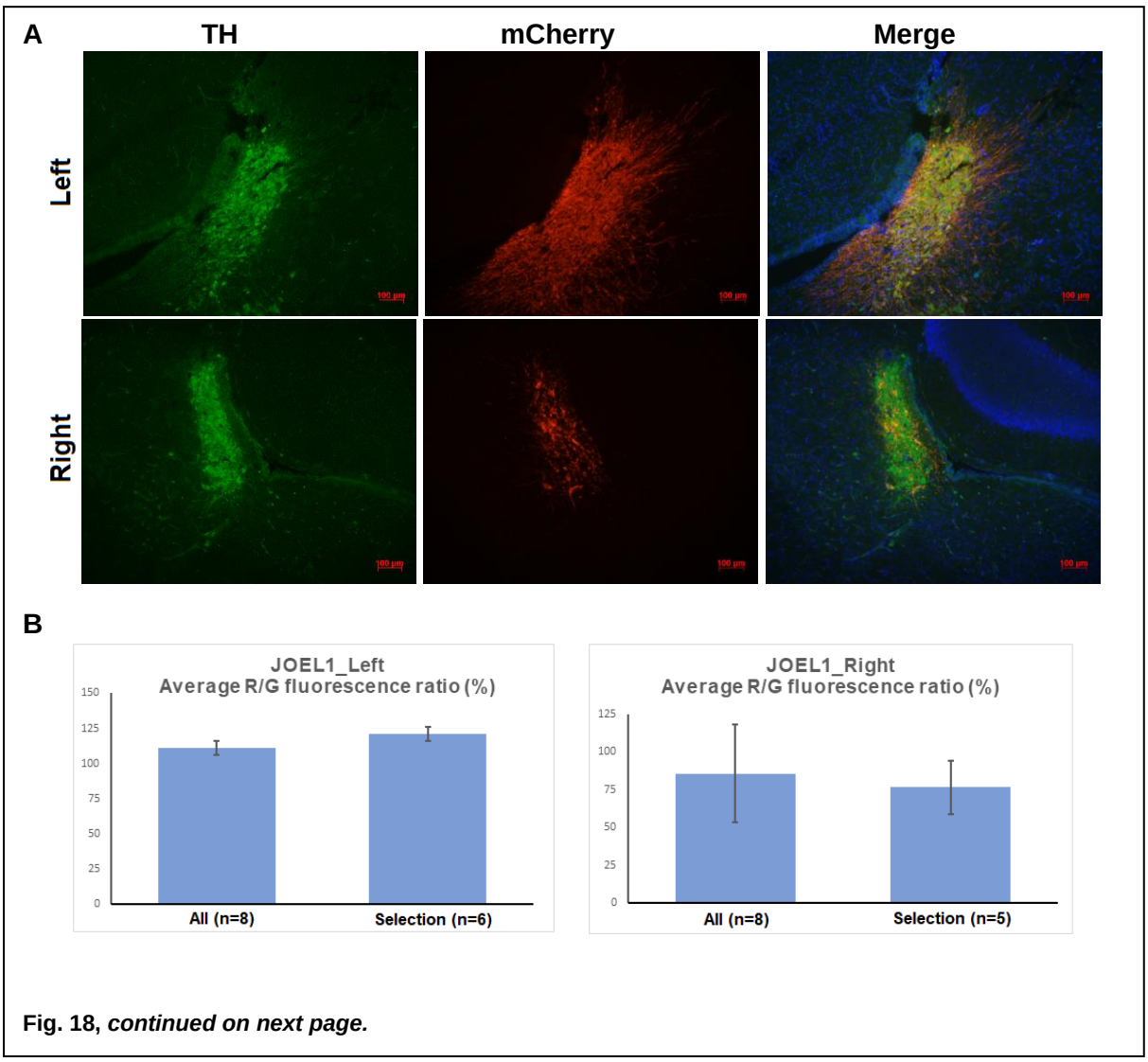

Fig. 18, ***continued on next page.***

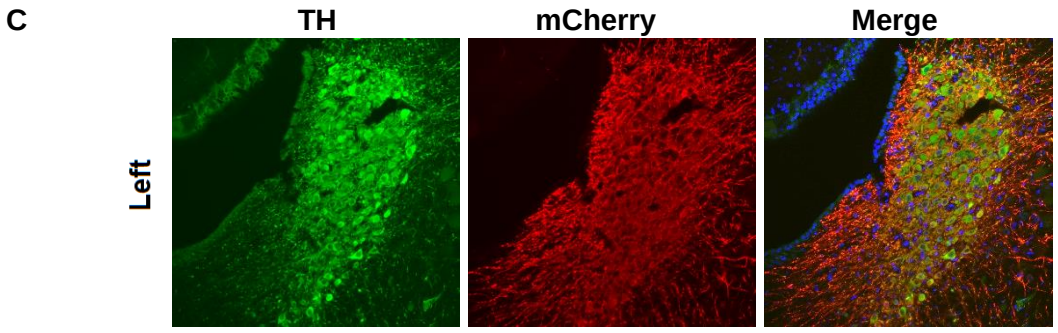

Fig. 18 Immunohistochemical results of JOEL1. **(A)** Upper images: left LC. Lower images: right LC. Left: tyrosine hydroxylase (TH) staining of LC neurons. Middle: mCherry expression indicating the expression of opsins in both LCs. Right: merged image of the TH, mCherry and DAPI staining. **(B)** Graphs of the ratios between red and green fluorescence, averaged over all immunofluorescence images (left bar) or over a selection of high quality images (right bar). **(C)** Images of the left LC acquired on a confocal microscope used for manual cell counting.

Stainings of the second animal (ID: JOEL3) showed low expression levels bilaterally. Only a couple of red fluorescent cells were present per LC on both sides **(Fig. 19 A)**. Based on qualitative assessment, these expression levels could be considered equally low. But with the quantitative approach, expression levels appear to be a bit higher on the left. Here, the average red/green ratio over all images was 29,71% (± 16,60%, n=7) and the ratio based on high quality images was 35,72% (± 15,95%, n=5). While on the right side, the respective ratios are 20,26% (± 7,99%, n=7) and 24,56% (± 3,81%, n=5). Manual cell counting on a confocal image of a LC on the left side yielded an expression level of 7,55% (4/53 double positive neurons), close to the expression level of 12,05% based on the red/green ratio **(Fig. 19 C)**.

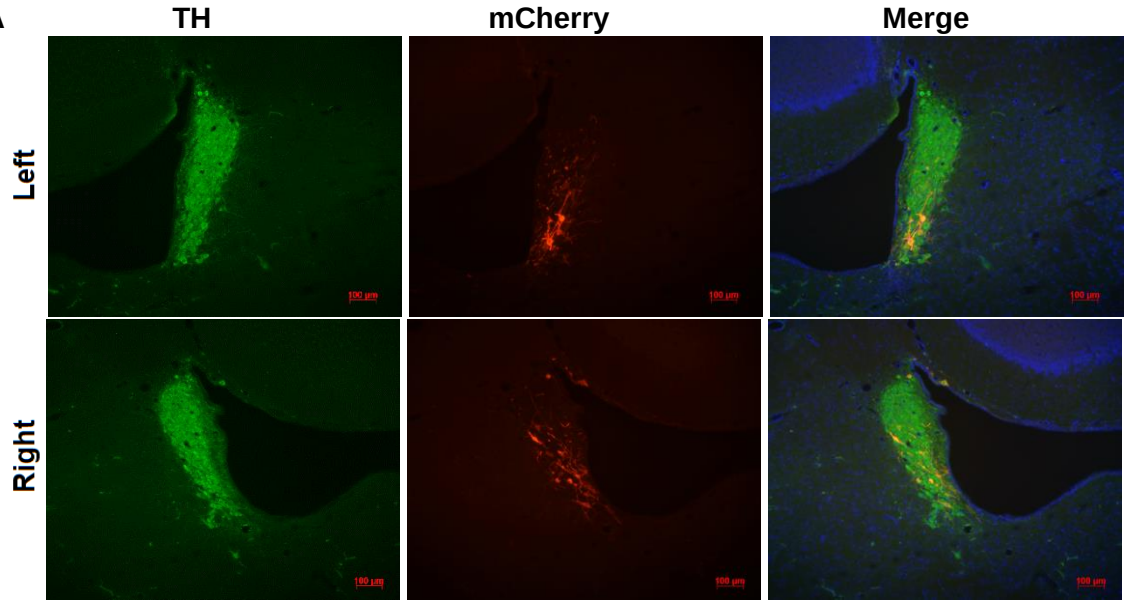

Fig. 19, ***continued on next page.***

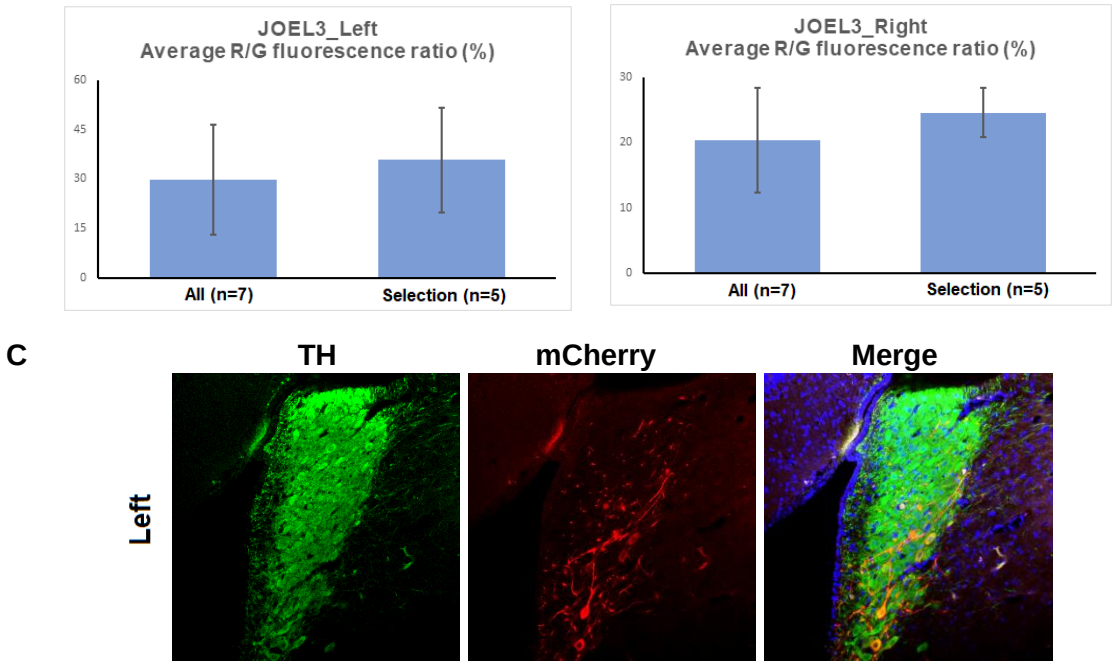

Fig. 19 Immunohistochemical results of JOEL3. **(A)** Upper images: left LC. Lower images: right LC. Left: tyrosine hydroxylase (TH) staining of LC neurons. Middle: mCherry expression indicating the expression of opsins in some LC neurons. Right: merged image of the TH, mCherry and DAPI staining. **(B)** Graphs of the ratios between red and green fluorescence, averaged over all immunofluorescence images (left bar) or over a selection of high quality images (right bar). **(C)** Images of the left LC acquired on a confocal microscope used for manual cell counting.

The third animal (ID: JOEL4) also had two successfully transduced nuclei. Here, the right LC displayed the highest amount of opsin expression as mCherry was more ubiquitously present while on the left side mCherry expression was mostly present in the ventral half of the LC **(Fig. 20 A)**. Quantitative measurements on images of the right side gave an overall average red/green ratio of 435,26% (± 679,22%, n=11). This excessive high ratio is caused by some images containing only a small part of the LC but a high amount of ventrally projecting axons. The average ratio based on only the best images was 176,05% (± 8,74%, n=4) on the other hand. The ratios of the images on the left were 153,99% (± 152,17%, n=11) when averaged over all images and 99,74% (± 46,10%, n=4) when based on high quality images. Cells were counted in one LC on the right side, resulting in an expression level of 92% (23/25 double positive neurons, **Fig. 20 C**). This was again more informative than the red/green ratio of 172,30% of this LC image.

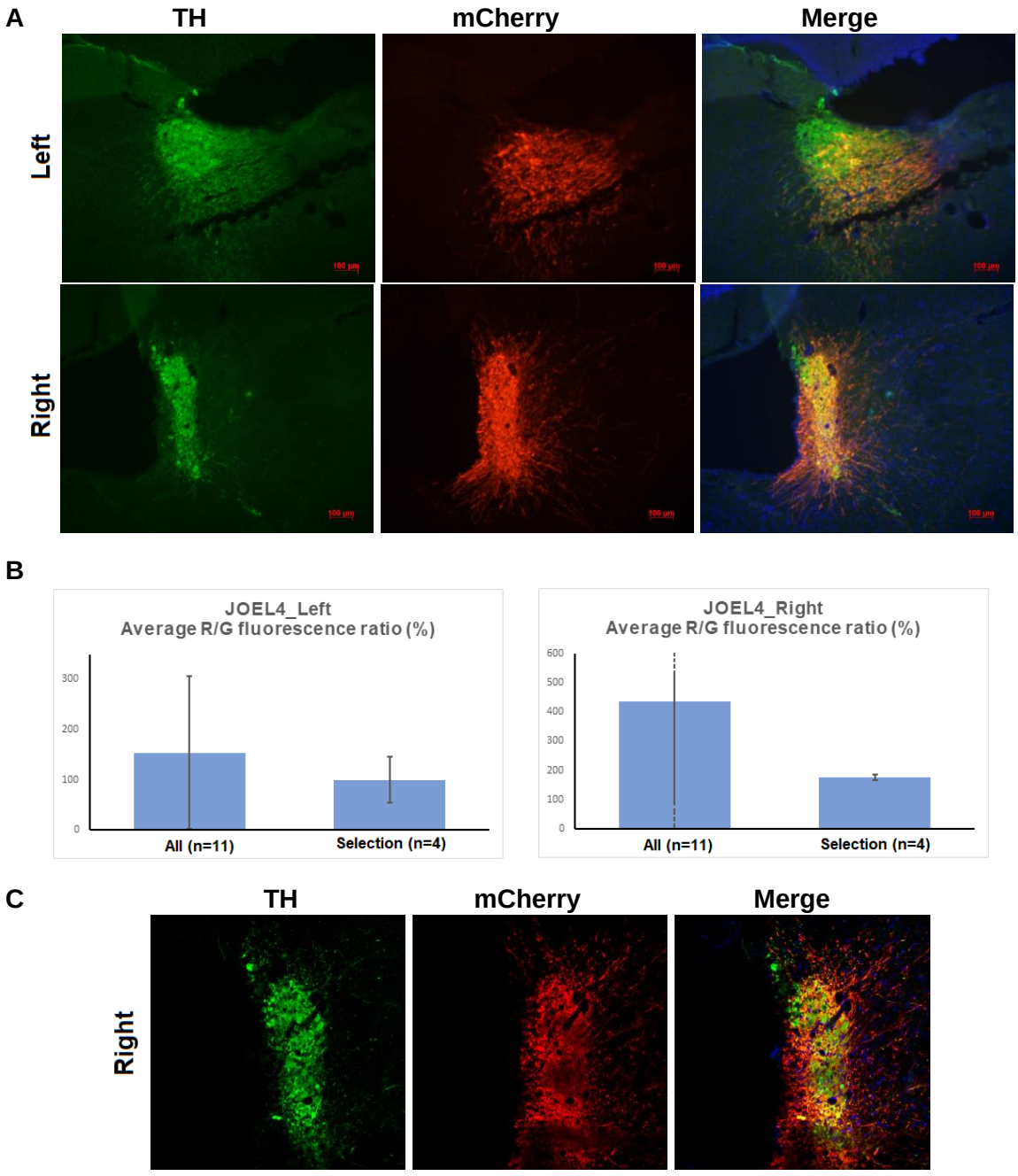

Fig. 20 Immunohistochemical results of JOEL4. **(A)** Upper images: left LC. Lower images: right LC. Left: tyrosine hydroxylase (TH) staining of LC neurons. Middle: mCherry expression indicating expression in both LCs, in the left LC more ventrally. Right: merged image of the TH, mCherry and DAPI staining. **(B)** Graphs of the ratios between red and green fluorescence, averaged over all immunofluorescence images (left bar) or over a selection of high quality images (right bar). **(C)** Images of the right LC acquired on a confocal microscope used for manual cell counting.

In contrast to the previous animals, the results in the last animal (ID: JOEL6) differed greatly between the left and right LC **(Fig. 21 A)**. On the left, the injection had clearly been successful and opsin expression was visible all over the LC. However, in the right LC only a minimal amount of LC neurons were labeled with mCherry. Quantification of the expression levels also clearly showed the difference between the two sides: on the left the average red/green fluorescence ratio was 190,57% (± 69,06%, n=9) for all images and 169,62% (± 71,36%, n=5)

for only the best images and on the right the overall average was 21,10% (± 14,84%, n=5) and the average of the best images was 15,86% (± 4,22%, n=2). Manual cell counting was performed on a confocal image of the left LC and showed an expression level of 82,14% (46/56 double positive neurons) while the red/green ratio was 99,57% **(Fig 21 C)**.

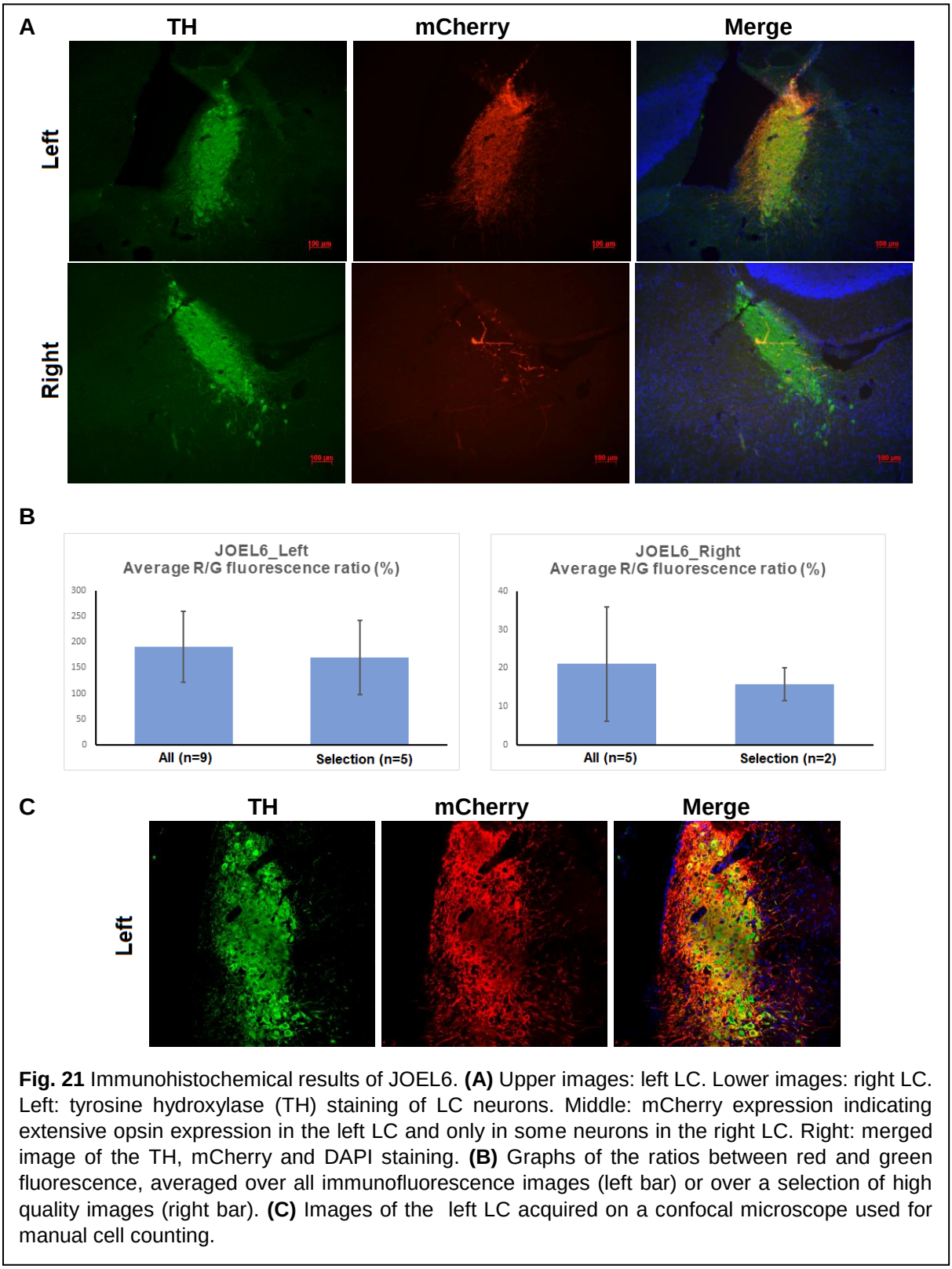

Fig. 21 Immunohistochemical results of JOEL6. **(A)** Upper images: left LC. Lower images: right LC. Left: tyrosine hydroxylase (TH) staining of LC neurons. Middle: mCherry expression indicating extensive opsin expression in the left LC and only in some neurons in the right LC. Right: merged image of the TH, mCherry and DAPI staining. **(B)** Graphs of the ratios between red and green fluorescence, averaged over all immunofluorescence images (left bar) or over a selection of high quality images (right bar). **(C)** Images of the left LC acquired on a confocal microscope used for manual cell counting.

3.1.5 Hippocampal projections

As a quick control, hippocampal slices were collected from the last set of animals and inspected after IHC staining for the presence of projections from LC neurons expressing mCherry. Images of one animal with successful LC transduction (JOEL4) could be collected on which noradrenergic axons were visible in the hippocampus **(Fig. 22 A)**. A few of these axons displayed red fluorescence, indicating that they originated from transduced LC neurons and that the opsins were also expressed on these processes **(Fig. 22 B-D)**.

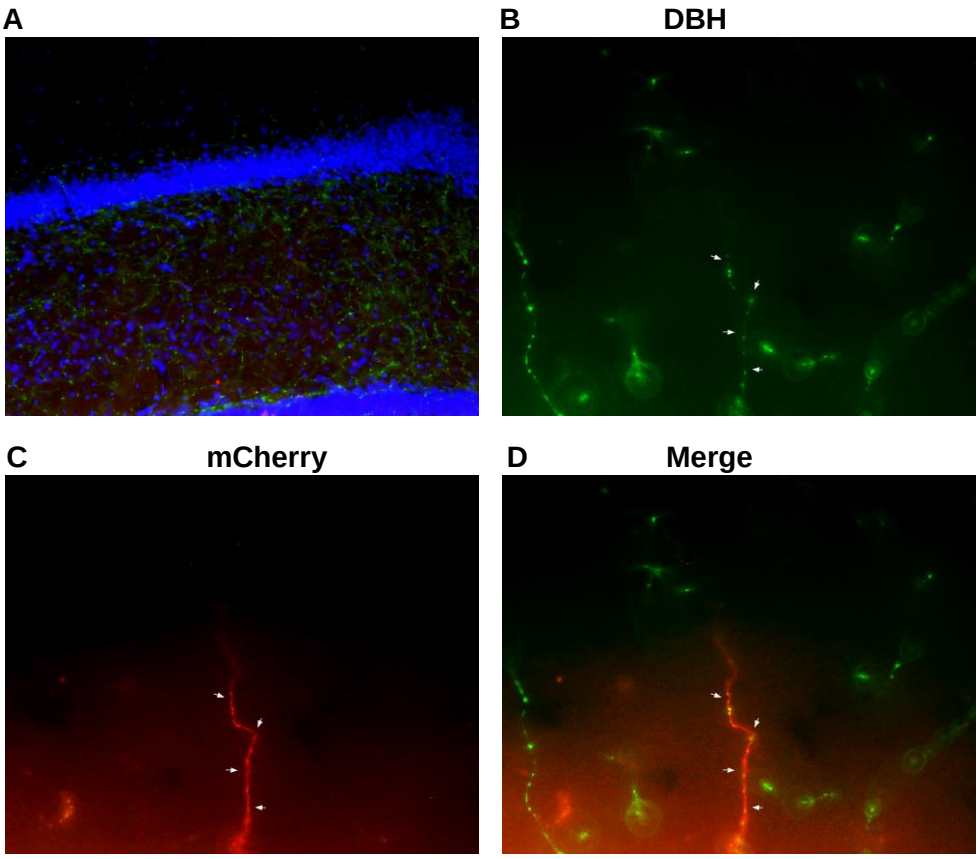

Fig. 22 Hippocampal slice of JOEL4. **(A)** Overview image of the area of the dentate gyrus containing a high amount of noradrenergic axons, visualized by dopamine β-hydroxylase (DBH) staining. **(B-D)** Close-up of the noradrenergic axons from the LC in the hippocampus. One axon is visible (marked with white arrows) that stains double positive for DBH **(B)** and mCherry **(C)**.

4. Discussion

The experiments performed during this thesis were limited to only the first phase of the project; the optimization and validation of opsin expression. This mainly due to the occurrence of more problems with achieving satisfying expression results than was foreseen. If the probability of having sufficient opsin expression needed to activate the LC in an animal is not high enough after injection, it is not justified to carry out further optogenetic experiments on animals. It was then also decided that there was need for a quantitative approach for the evaluation of expression levels. Unfortunately, this led to extra work and left no time for the execution of any following experiments in the limited duration of this thesis.

4.1 Validation/optimization of opsin expression

Although the pilot trial showed promising results, with 3 out of 3 animals displaying successful transduction of the LC, the variability in expression levels of the following experiments are proof of how challenging it can be to achieve this consistently. In the first set of animals there was a low success rate with loss of 2 rats during surgery and only 2 out of 6 injections leading to successful transduction of the LC similar to that of the animals from the pilot experiment. Of the 4 rats in which transduction failed, 2 did show some signs of mCherry on axons running though the LC. This indicates that there must have been a very small number of cells that did express the opsin in a different part of the LC. It was also the aim in this first experiment to investigate if the implantation of an optical fiber directly following the injection of viral vector impacted transgene expression. However, due to the low success rate both in the group of animals with and without a fiber, no information regarding this question could be gained. But some valuable information was obtained by looking at the histological results of one animal, namely the fact that the optical fiber was implanted too deeply. Optical fibers should be placed above the LC for illumination but in this case the fiber was inserted into the LC, causing damage. Knowing this, the dorsoventral coordinates for future fiber implantations were slightly changed. But in fact, the depth of implantation could be chosen even more superficial while still retaining sufficient illumination. In the study of Hickey et al. for example, optoactivation of the LC was obtained with fibers only inserted up to 300 µm into the brain tissue while the LC was located at a depth of >500 µm [46].

As it was clear more testing of the injection procedure was needed, a second set of animals was used. In this experiment injections were made bilaterally to increase the number of test sites while keeping the number of animals used to a minimum. As one rat died during surgery and fixation of the brain tissue of one of the 5 injected rats failed, the results of 4 animals that were bilaterally injected remained. In these 4 rats, 5 out of 8 injections had led to successful transduction of the targeted LC's. This was a substantial improvement compared to the low success rate of 2/6 in the first experiments and can be considered an acceptable rate of success for starting further optogenetic experiments.

Yet there were no changes made in the injection procedures between these two sets of experiments that could explain the increased success rate. This was also not deemed necessary as the procedure used to target the LC is a validated procedure, both based on previous experiences in our lab as on studies from other groups working on the LC. For example, the stereotaxic coordinates used here to target the LC (AP -3.9mm, ML ±1.15mm relative to Lambda) are very similar to the coordinates used by the group of Aston-Jones (AP -3.8mm, ML ±1.3mm relative to Lambda), as they also injected adult rats weighing more than 300g [47]. Furthermore, injections were also performed as described by this group; with the nose of the animals lowered to reposition Bregma 2mm below Lambda to obtain a rostral angulation of 15° so the transverse sinus can be avoided [48]. One point of difference with the procedure used by the group of Aston-Jones is the instrument used for injections. In their experiments, vectors are delivered through a glass micropipette with brief pneumatic pulses

using a Picospritzer III (Parker Instruments) while we used a Hamilton syringe. But this syringe is also commonly used by other researchers for the same purposes, as reported for example in a recent study on optogenetic LC modulation by Glennon et al. [49]. So that small difference in the injection procedure is most likely insignificant. However, the main difference with the group of Aston-Jones are the DV coordinates used. To determine the depth of injections, they first verify the location of the LC through unit recordings (based on specific electrophysiological characteristics of LC neurons). This led to DV coordinates between 5.6-6.8mm in one of their studies [48]. This depth is not much different from the 5.3-5.8mm used in our experiments. However this was in rats weighing 250-300g while our rats weighed at least 350g. In their work on rats weighing >300g, injections in the LC after localization had to be performed more deeply at 6.5-7.0mm DV [47]. These differences in DV location indicate that it might be worthwhile to also rely on unit recording prior to injections in future experiments. The depth and volume of injections in our experiments (3 injections of 300 nl each at -5.8, -5.5 and -5.3mm relative to dura) were based on those used by the group of Pickering, since they supplied the viral vector. This group does use different AP/ML coordinates and a 10° rostral angulation for targeting the LC, but also work in smaller rats ranging 120-300g in weight [43, 46, 50]. So it might be that these DV coordinates are not always optimal for use in larger animals, which could partially explain the varying success in this project.

Personal experience of the experimenter performing the injections could also have an influence on the success rate; performing the procedure multiple times would improve the success rate through practice and could explain the difference between the first and second set of experiments. However, for these experiments this was not the case as the two sets of injections were performed by two different experimenters. The difference between the two groups probably just indicates the variability that is present due to the difficulty of the injection procedure for the transduction of LC. When the results of the two groups of rats are pooled, we get a 50% success rate with 7 out of the 14 targeted LC's possessing high levels of opsin expression. This rate of success is not unusual for experiments focusing on the LC and can also be found in literature. For example, in a recent study on chemogenetic LC activation Rorabaugh et al. reported that 80% of their bilaterally injected animals displayed only unilateral DREADD expression [51]. Bilaterally injections were performed in 29 rats, which means that 23 out of 58 injections failed. This corresponds to a success rate of 35 out of 58 or 60%, not much different from the success rate of our experiments.

In their article, Rorabaugh et al. mention that the reason for these problems is "most likely due to difficulties targeting a deep brainstem nucleus of such small dimensions" [51]. The anatomy of the LC indeed makes it a very challenging subject to work on. Its small size leaves little room for error when targeting the LC based on stereotaxic coordinates. Slight deviations can lead to the needle of the syringe completely missing the LC, resulting in a failed injection. Since the coordinates for targeting the LC in our experiments are based on the coordinates of Lambda (for AP and ML) and the dura mater (for DV) -and these reference points are not always clearly measurable during surgery- misreading these coordinates could be one of the reasons some injections failed in certain animals. Depending then on how much the injection was off-target, opsin expression can be completely absent (such as in LSO2 and LSO3) or only a small amount of vector could have diffused into the LC resulting in very low expression (such as in LSO6 and LS7). In case of bilateral injections, misreading the coordinates of the reference points could explain both injections ending up unsuccessful, as seen in the second animal (JOEL3).

Besides the difficulties with targeting the LC, other problems during the injection procedure can occur that could have caused the variability in success. For example, storage of the viral vector on ice during multiple days of surgeries could be insufficient and cause the vector to

lose some if its efficacy. According to virus handling and storage guidelines, viral vectors should be kept at -80°C for longtime storage and can only be preserved at higher temperatures for limited amounts of time. Transduction efficiency has been found to decrease after a couple of days when stored at -20°C and after only one day when stored at 4°C [52]. However, in these experiments the last animals to undergo surgery have had successful transductions, making it an unlikely explanation in this case. A more probable cause is the occasional bleeding that occurred when a blood vessel or sinus was hit during the lowering of the needle into the brain. This happened in multiple animals and blood clots could have interfered with the outflow and diffusion of the viral vector. This could explain some of the within-animal variability encountered with the bilateral injections (e.g. JOEL6), where the first injection could have went without any problems but the second time the syringe could have been somewhat obstructed.

Now, with the main problem of transducing the LC mostly being the targeting itself, there will always be a chance that a part of the injections fail. There is no real way to get around this when attempting to transduce the LC via a viral vector. But there exists the option to work with transgenic animals for chemo- or optogenetic modulation of LC. As an example, Wang et al. used the Cre/loxP recombinase system to express ChR2 in the LC of mice [53]. Mice carrying the ChR2 gene preceded by a loxP-flanked STOP cassette were crossed with TH-Cre mice, resulting in offspring that expressed ChR2 in the TH^+ neurons of the LC. With this method, no surgical procedures are required to obtain opsin expression in the desired neuron population and the same technique can be performed on rats as there is a transgenic TH-Cre rat line available [54]. However, there is a considerable higher amount of time and cost associated with working with transgenic animals. For this reason, transduction via viral vector is still considered an acceptable approach for modulation of the LC, even with an intermediate success rate.

4.2 Quantification of expression levels

After performing the injections and obtaining the histological results, the second major part of this thesis became the quantification of opsin expression on these results. Several different approaches for the reporting of expression results can be found in literature on chemo- or optogenetic modulation of LC. In some articles, expression is only qualitatively evaluated based on IHC. This is the case for example in two articles on optogenetic stimulation of LC neurons. In the study of Hickey et al. expression of ChR2 in the LC was verified on images obtained on a conventional fluorescence microscope and reported as “robust, selective expression” [46]. Similarly, in an article of Wang et al. ChR2 expression is also simply expressed as “punctate and robust expression”, but here this was examined on confocal images [53]. Although it is possible to assess the success of viral vector injections in a qualitative way and make a distinction between nuclei with high, intermediate or low expression levels, a quantitative analysis makes it possible to report results more objectively. It also enables the use of expression criteria in case of results with intermediate expression levels. A cut-off value can be set to decide whether or not the results of an animal are taken into account during analysis. For example, in a study by Vazey et al., subjects needed to meet expression criteria of >60% LC coverage to be taken into account [47]. So by quantifying expression levels and determining a threshold in advance, selection bias can be avoided.

Once the decision to perform a quantitative analysis was made, a method had to be found to do this. The ideal way to quantify expression is to perform cell counting on IHC stainings and look at every neuron that stains positive for TH, mCherry or both, as is done by most research groups that include quantitative expression results in their articles [43, 55] . By doing this on several slices spread over the anterior-posterior axis of the LC, a representative expression level can be calculated. Such cell counting is commonly performed on images acquired by confocal microscopy, as on these images most cell bodies lying in the confocal plane can be

clearly distinguished. It is then also possible to set certain criteria to determine whether a cell should be counted or not. For example, in the article of Howorth et al. it is reported that noradrenergic neurons were only counted when the nucleus could be identified in the cell body and when a primary dendrite was visible [56].

Unfortunately, for this thesis the time that could be spend using a confocal microscope was limited and only one image per animal could be taken. So the quantification on the few confocal images served more as a proof of concept. But since plenty of images obtained on an epifluorescence microscope were available, quantitative analysis was mainly performed on these. At first, manual cell counting was attempted on these images but it soon became clear this did not yield reliable results. Most cells were not clearly distinguishable and when cell counts were performed by two different experimenters the results could differ greatly. This indicated that this approach was too subjective and it was then opted to use the ratio of red/green fluorescence to define the expression levels in a more objective manner.

By measuring the amount of red fluorescent signal and comparing this to the amount of green fluorescence, the level of LC that was covered by opsin expression could be gauged. This was easily done using ImageJ software and was less labor intensive compared to cell counting. But this method of quantification has some disadvantages. As all the pixels with an intensity above the chosen threshold were counted, fluorescent signals caused by artefacts on the slice were sometimes also included, skewing the result. This problem could be mostly avoided by making a selection of only the best images. The main problem of this method however is the fact that it is not always very representative of the actual expression level. This is because the red fluorescent signal, indicating the presence of mCherry, is both clearly present on neuronal cell bodies and on axons while green fluorescence is mostly coming from the cell bodies and not as much from neuronal processes. In case of successful transduction of the LC, this made red/green fluorescence ratios often exceed 100% and rendered them not very informative, whereas in the case of cell counting an expression level of >100% would indicate overexpression of the opsin in non-noradrenergic neurons.

As previously mentioned, cell counting on confocal images was limited to one image for each animal. The resulting expression level was thus not representative for the entire subject, but it did allow for a comparison between the two quantification methods which gave proof of the superiority of cell counting. The biggest difference was visible in subjects with very high opsin expression where, as mentioned above, red/green fluorescence ratios exceeded 100% by far (e.g. 165,35% for LSO1) while cell counting revealed a more realistic expression level below 100% (e.g. 90% for LSO1). And on the opposite side, in case of very low expression, cell counting could verify that on a specific slice the expression level was 0%, because not a single neuron on the image expressed mCherry, while the red/green ratio did pick up some red fluorescence from axons resulting in an expression level >0% (e.g. 4,62% for LSO6). On slices with more moderate expression levels (not very high and not very low) the difference between the two methods was smaller, but cell counting delivered a more nuanced result. For example, on the image of animal JOEL1 the expression level based on the ratio was 99,53%, but the expression level after cell counting was 89,47%. Besides enabling a more accurate measurement of expression levels, the images from the confocal microscope were also useful for inspecting any possible off-target expression. Because of the high resolution, it was easy to spot any non-noradrenergic neurons expressing mCherry. But these were not present on any of the pictures, indicating that the viral vector worked as intended and only led to opsin expression in the desired noradrenergic neurons. This is consistent with the reports of the group of Pickering which uses the same CAV2-PRS-ChR2-mCherry vector, where fluorescence is also restricted to DBH+ neurons, indicating the selectivity of the PRS promoter [43].

While the results from the cell counting proof that this is a more optimal way of quantifying expression, it must be noted that an even more correct method can be found in literature: a design-based stereological analysis using the optical fractionator method [57]. This is a method developed to estimate the number of cells in a region of interest with as little bias as possible. Neurons are counted according to certain criteria in unbiased virtual counting spaces in a series of systemically and randomly sampled sections. The number of counted neurons is then multiplied with a factor (dependent on the number and height of sections) to obtain an estimation of the total number of cells [58]. This method has been used in recent studies by groups working on chemogenetic modulation of LC to obtain unbiased cell counts [50, 51]. This does require specific computer-interfaced microscopes with specialized software, since these were not available this method could not be applied in this project. It might also be sufficient to perform manual cell counting as was done for this thesis, which is less costly and time-consuming, as it is also commonly performed by other research groups. But first it should then be determined how biased this manual cell counting is by comparing the results of different experimenters counting the same images.

5. Conclusion

Optogenetic modulation of the LC via stereotaxic injection of a viral vector is a challenging procedure. The CAV2-PRSx8-ChR2-mCherry vector that is being used performs well, the greatest difficulty lies in targeting this small nucleus. If this is done successfully, vector injections lead to satisfactory opsins expression levels. The success rate obtained over all the experiments of this thesis equals 50%, which is a moderate amount but not uncommon based on literature. It might be possible to increase this rate of success by adopting unit recordings into the injection procedure to verify the location of the LC, as mentioned previously. Alternatively, the difficulties associated with targeting this small nucleus could be circumvented by making use of a retrograde targeting strategy. This would be similar to how the group of Pickering used the ability of the CAV2 vector to transduce neurons via retrograde axonal transport to optogenetically modulate pontospinal LC neurons [43]. Injecting the CAV2 vector into the hippocampus should lead to transduction of the LC neurons projecting to this brain region. Because the aim of this project is to examine the effect of LC on hippocampal activity, optogenetic modulation of those specific noradrenergic neurons should suffice. Performing injections into the hippocampus should be easier compared to the LC and should theoretically increase the rate of success.

Besides some further optimization of the injection procedure, some more validation experiments can be considered for the future. One of the things that needs to be examined is the influence of the optical fiber implantation on opsin expression, which could not be determined in this project because of the low success rate in the first set of rats. As mentioned previously, a more superficial implantation of the fibers is possible to avoid damage to the LC. If opsin expression remains unaffected, a next step would be checking if illumination of the transduced LC leads to the expected neuronal activation. This can be done by performing c-fos stainings after illumination (the immediate early gene c-fos is expressed in neurons after neuronal activity, [59]). This is a commonly used validation step, described for example in the articles on chemogenetic LC modulation by Rorabaugh et al. and by Cope et al. [48, 51].

Once this is all validated, the planned experiments on hippocampal excitability can be started. Quantification of expression levels will also be necessary for the analysis of any future results. For this, cell counting on confocal images would be the optimal approach, as was illustrated in this project.

6. References

1. Behr C, Goltzene MA, Kosmalski G, Hirsch E, Ryulin P (2016) Epidemiology of epilepsy. *Rev Neurol* **172**: 27-36
2. Scheffer IE, Berkovic S, Capovilla G, Connolly MB, French J, Guilhoto L, Hirsch E, Jain S, Mathern GW, Moshe SL*, et al.* (2017) ILAE classification of the epilepsies: Position paper of the ILAE Commission for Classification and Terminology. *Epilepsia* **58**: 512-521
3. Stafstrom CE, Carmant L (2015) Seizures and epilepsy: an overview for neuroscientists. *Cold Spring Harb Perspect Med* **5**
4. Sander JW (2003) The epidemiology of epilepsy revisited. *Current Opinion in Neurology* **16**: 165-170
5. Kwan P, Brodie MJ (2000) Early identification of refractory epilepsy. *The New England journal of medicine* **342**: 314-9
6. Beekwilder JP, Beems T (2010) Overview of the Clinical Applications of Vagus Nerve Stimulation. *J Clin Neurophysiol* **27**: 130-138
7. Cimpianu CL, Strube W, Falkai P, Palm U, Hasan A (2017) Vagus nerve stimulation in psychiatry: a systematic review of the available evidence. *J Neural Transm* **124**: 145-158
8. Ekmekci H, Kaptan H (2017) Vagus Nerve Stimulation. *Open Access Maced J Med Sci* **5**: 391-394
9. Giordano F, Zicca A, Barba C, Guerrini R, Genitori L (2017) Vagus nerve stimulation: Surgical technique of implantation and revision and related morbidity. *Epilepsia* **58 Suppl 1**: 85-90
10. Heck C, Helmers SL, DeGiorgio CM (2002) Vagus nerve stimulation therapy, epilepsy, and device parameters - Scientific basis and recommendations for use. *Neurology* **59**: S31-S37
11. Ben-Menachem E, Revesz D, Simon BJ, Silberstein S (2015) Surgically implanted and non-invasive vagus nerve stimulation: a review of efficacy, safety and tolerability. *Eur J Neurol* **22**: 1260-8
12. Panebianco M, Zavanone C, Dupont S, Restivo DA, Pavone A (2016) Vagus nerve stimulation therapy in partial epilepsy: a review. *Acta Neurol Belg* **116**: 241-8
13. Fornai F, Ruffoli R, Giorgi FS, Paparelli A (2011) The role of locus coeruleus in the antiepileptic activity induced by vagus nerve stimulation. *Eur J Neurosci* **33**: 2169-78
14. De Herdt V, Boon P, Ceulemans B, Hauman H, Lagae L, Legros B, Sadzot B, Van Bogaert P, Van Rijckevorsel K, Verhelst H*, et al.* (2007) Vagus nerve stimulation for refractory epilepsy: A Belgian multicenter study. *Eur J Paediatr Neurol* **11**: 261-269
15. George MS, Nahas Z, Bohning DE, Mu QW, Kozel FA, Borckhardt J, Denslow S (2004) Mechanisms of action of vagus nerve stimulation (VNS). *Clin Neurosci Res* **4**: 71-79
16. Berridge CW, Waterhouse BD (2003) The locus coeruleus-noradrenergic system: modulation of behavioral state and state-dependent cognitive processes. *Brain research Brain research reviews* **42**: 33-84
17. Swanson LW (1976) The locus coeruleus: a cytoarchitectonic, Golgi and immunohistochemical study in the albino rat. *Brain research* **110**: 39-56
18. Holets VR, Hokfelt T, Rokaeus A, Terenius L, Goldstein M (1988) Locus coeruleus neurons in the rat containing neuropeptide Y, tyrosine hydroxylase or galanin and their efferent projections to the spinal cord, cerebral cortex and hypothalamus. *Neuroscience* **24**: 893-906
19. Schwarz LA, Luo L (2015) Organization of the locus coeruleus-norepinephrine system. *Curr Biol* **25**: R1051-r1056
20. Strosberg AD (1993) Structure, function, and regulation of adrenergic receptors. *Protein Sci* **2**: 1198-209
21. Aston-Jones G, Bloom FE (1981) Activity of norepinephrine-containing locus coeruleus neurons in behaving rats anticipates fluctuations in the sleep-waking cycle. *The Journal of neuroscience : the official journal of the Society for Neuroscience* **1**: 876-86
22. Aston-Jones G, Bloom FE (1981) Norepinephrine-containing locus coeruleus neurons in behaving rats exhibit pronounced responses to non-noxious environmental stimuli. *The Journal of neuroscience : the official journal of the Society for Neuroscience* **1**: 887-900

23. Sara SJ (2009) The locus coeruleus and noradrenergic modulation of cognition. *Nature reviews Neuroscience* **10**: 211-23
24. Krahl SE, Clark KB, Smith DC, Browning RA (1998) Locus coeruleus lesions suppress the seizure-attenuating effects of vagus nerve stimulation. *Epilepsia* **39**: 709-714
25. Dorr AE, Debonnel G (2006) Effect of vagus nerve stimulation on serotonergic and noradrenergic transmission. *J Pharmacol Exp Ther* **318**: 890-8
26. Roosevelt RW, Smith DC, Clough RW, Jensen RA, Browning RA (2006) Increased extracellular concentrations of norepinephrine in cortex and hippocampus following vagus nerve stimulation in the rat. *Brain Res* **1119**: 124-32
27. Dalton JC, Roberts DC, McIntyre DC (1985) Supersensitivity to the anticonvulsant and proconvulsant activity of clonidine following noradrenaline depletion induced by 6-hydroxydopamine. *Psychopharmacology (Berl)* **85**: 319-22
28. Giorgi FS, Pizzanelli C, Biagioni F, Murri L, Fornai F (2004) The role of norepinephrine in epilepsy: from the bench to the bedside. *Neurosci Biobehav Rev* **28**: 507-24
29. Corcoran ME, Mason ST (1980) Role of forebrain catecholamines in amygdaloid kindling. *Brain research* **190**: 473-84
30. Larsen LE, Van Lysebettens W, Germonpre C, Carrette S, Daelemans S, Sprengers M, Thyrion L, Wadman WJ, Carrette E, Delbeke J*, et al.* (2017) Clinical Vagus Nerve Stimulation Paradigms Induce Pronounced Brain and Body Hypothermia in Rats. *Int J Neural Syst* **27**: 13
31. Larsen LE, Wadman WJ, van Mierlo P, Delbeke J, Grimonprez A, Van Nieuwenhuyse B, Portelli J, Boon P, Vonck K, Raedt R (2016) Modulation of Hippocampal Activity by Vagus Nerve Stimulation in Freely Moving Rats. *Brain Stimul* **9**: 124-132
32. Whishaw IQ, Vanderwolf CH (1971) Hippocampal EEG and behavior: effects of variation in body temperature and relation of EEG to vibrissae movement, swimming and shivering. *Physiol Behav* **6**: 391-7
33. Sternson SM, Roth BL (2014) *Chemogenetic Tools to Interrogate Brain Functions*. In Annual Review of Neuroscience, Vol 37, Hyman SE (ed) Palo Alto: Annual Reviews
34. Coward P, Wada HG, Falk MS, Chan SD, Meng F, Akil H, Conklin BR (1998) Controlling signaling with a specifically designed Gi-coupled receptor. *Proc Natl Acad Sci U S A* **95**: 352-7
35. Bn A, Roth B (2005) *Creation of designer biogenic amine receptors via directed molecular evolution*.
36. Magnus CJ, Lee PH, Atasoy D, Su HH, Looger LL, Sternson SM (2011) Chemical and genetic engineering of selective ion channel-ligand interactions. *Science* **333**: 1292-6
37. Fenno L, Yizhar O, Deisseroth K (2011) The development and application of optogenetics. *Annu Rev Neurosci* **34**: 389-412
38. Nagel G, Szellas T, Huhn W, Kateriya S, Adeishvili N, Berthold P, Ollig D, Hegemann P, Bamberg E (2003) Channelrhodopsin-2, a directly light-gated cation-selective membrane channel. *Proc Natl Acad Sci U S A* **100**: 13940-5
39. Boyden ES, Zhang F, Bamberg E, Nagel G, Deisseroth K (2005) Millisecond-timescale, genetically targeted optical control of neural activity. *Nat Neurosci* **8**: 1263-8
40. Gradinaru V, Thompson KR, Deisseroth K (2008) eNpHR: a Natronomonas halorhodopsin enhanced for optogenetic applications. *Brain Cell Biol* **36**: 129-39
41. Airan RD, Thompson KR, Fenno LE, Bernstein H, Deisseroth K (2009) Temporally precise in vivo control of intracellular signalling. *Nature* **458**: 1025-9
42. Stevens L, Vonck K, Van Lysebettens W, Baekelandt V, Van Den Haute C, Carrette E, Boon P, Raedt R (2019) Genetic modification of Locus Coeruleus NE cells for chemogenetic activation remains challenging. *Frontiers in Neuroscience*
43. Li Y, Hickey L, Perrins R, Werlen E, Patel AA, Hirschberg S, Jones MW, Salinas S, Kremer EJ, Pickering AE (2016) Retrograde optogenetic characterization of the pontospinal module of the locus coeruleus with a canine adenoviral vector. *Brain research* **1641**: 274-90
44. Junyent F, Kremer EJ (2015) CAV-2—why a canine virus is a neurobiologist's best friend. *Current Opinion in Pharmacology* **24**: 86-93

45. Hwang DY, Carlezon WA, Jr., Isacson O, Kim KS (2001) A high-efficiency synthetic promoter that drives transgene expression selectively in noradrenergic neurons. *Human gene therapy* **12**: 1731-40
46. Hickey L, Li Y, Fyson SJ, Watson TC, Perrins R, Hewinson J, Teschemacher AG, Furue H, Lumb BM, Pickering AE (2014) Optoactivation of locus ceruleus neurons evokes bidirectional changes in thermal nociception in rats. *The Journal of neuroscience : the official journal of the Society for Neuroscience* **34**: 4148-60
47. Vazey EM, Moorman DE, Aston-Jones G (2018) Phasic locus coeruleus activity regulates cortical encoding of salience information. *Proc Natl Acad Sci U S A* **115**: E9439-e9448
48. Cope ZA, Vazey EM, Floresco SB, Aston Jones GS (2019) DREADD-mediated modulation of locus coeruleus inputs to mPFC improves strategy set-shifting. *Neurobiol Learn Mem* **161**: 1-11
49. Glennon E, Carcea I, Martins ARO, Multani J, Shehu I, Svirsky MA, Froemke RC (2019) Locus coeruleus activation accelerates perceptual learning. *Brain research* **1709**: 39-49
50. Hirschberg S, Li Y, Randall A, Kremer EJ, Pickering AE (2017) Functional dichotomy in spinal- vs prefrontal-projecting locus coeruleus modules splits descending noradrenergic analgesia from ascending aversion and anxiety in rats. *eLife* **6**
51. Rorabaugh JM, Chalermpalanupap T, Botz-Zapp CA, Fu VM, Lembeck NA, Cohen RM, Weinshenker D (2017) Chemogenetic locus coeruleus activation restores reversal learning in a rat model of Alzheimer's disease. *Brain*
52. Xu R, Rahimi M, Ma H, Fung P, Chang C, Xu S, During M (2005) Stability of infectious recombinant adeno-associated viral vector in gene delivery. *Med Sci Monit* **11**: Br305-8
53. Wang X, Pinol RA, Byrne P, Mendelowitz D (2014) Optogenetic stimulation of locus ceruleus neurons augments inhibitory transmission to parasympathetic cardiac vagal neurons via activation of brainstem alpha1 and beta1 receptors. *The Journal of neuroscience : the official journal of the Society for Neuroscience* **34**: 6182-9
54. Liu Z, Brown A, Fisher D, Wu Y, Warren J, Cui X (2016) Tissue Specific Expression of Cre in Rat Tyrosine Hydroxylase and Dopamine Active Transporter-Positive Neurons. *PLoS One* **11**: e0149379
55. Carter ME, Yizhar O, Chikahisa S, Nguyen H, Adamantidis A, Nishino S, Deisseroth K, de Lecea L (2010) Tuning arousal with optogenetic modulation of locus coeruleus neurons. *Nat Neurosci* **13**: 1526-33
56. Howorth PW, Teschemacher AG, Pickering AE (2009) Retrograde adenoviral vector targeting of nociresponsive pontospinal noradrenergic neurons in the rat in vivo. *J Comp Neurol* **512**: 141-57
57. West MJ, Slomianka L, Gundersen HJG (1991) UNBIASED STEREOLOGICAL ESTIMATION OF THE TOTAL NUMBER OF NEURONS IN THE SUBDIVISIONS OF THE RAT HIPPOCAMPUS USING THE OPTICAL FRACTIONATOR. *Anat Rec* **231**: 482-497
58. Schmitz C, Hof PR (2005) Design-based stereology in neuroscience. *Neuroscience* **130**: 813-31
59. Perrin-Terrin AS, Jeton F, Pichon A, Frugiere A, Richalet JP, Bodineau L, Voituron N (2016) The c-FOS Protein Immunohistological Detection: A Useful Tool As a Marker of Central Pathways Involved in Specific Physiological Responses In Vivo and Ex Vivo. *J Vis Exp*

Addendum

1. Protocol red/green fluorescence ratio in ImageJ

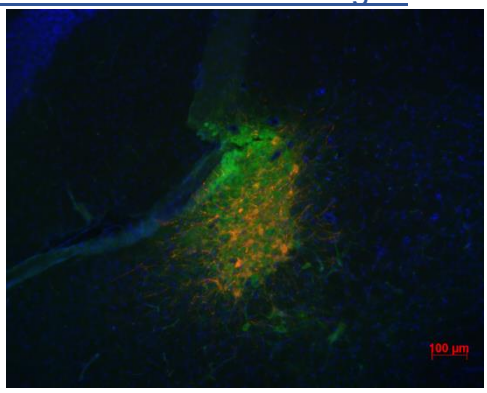

- **Open green and red channel in ImageJ**

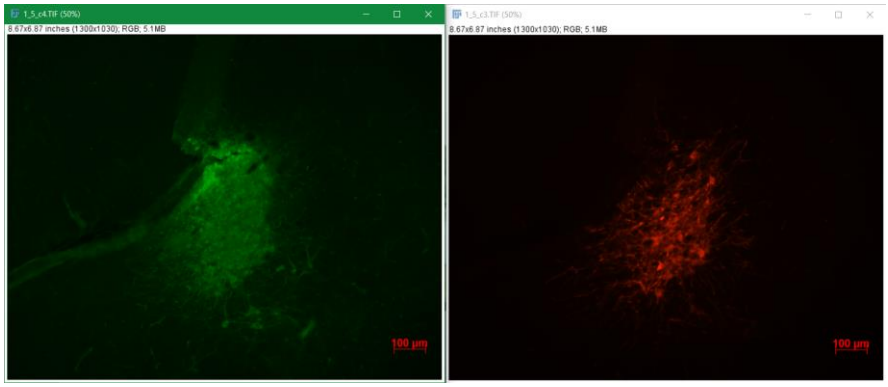

- **Change image type to 8-bit (grayscale)**

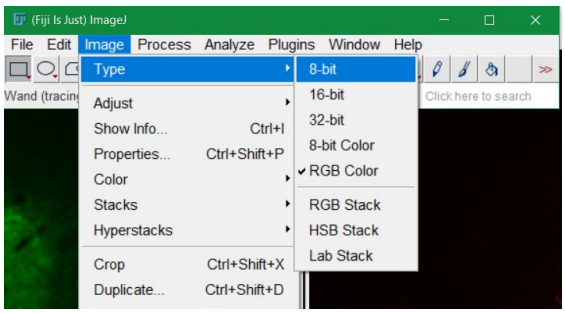

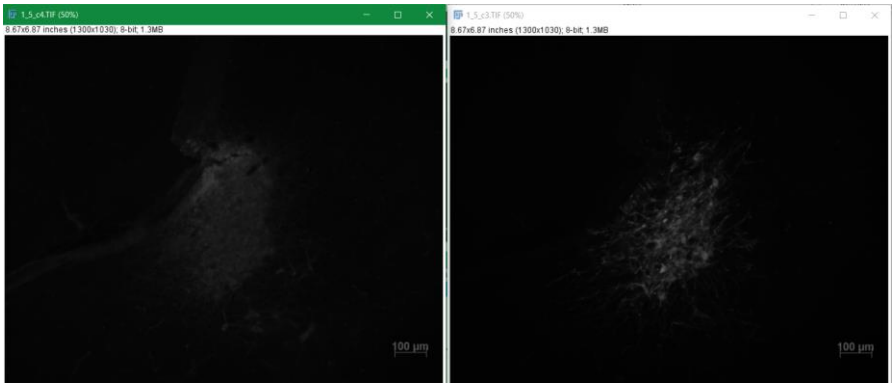

- **Open *Threshold* function to separate low intensity (background) signal from high intensity signal**

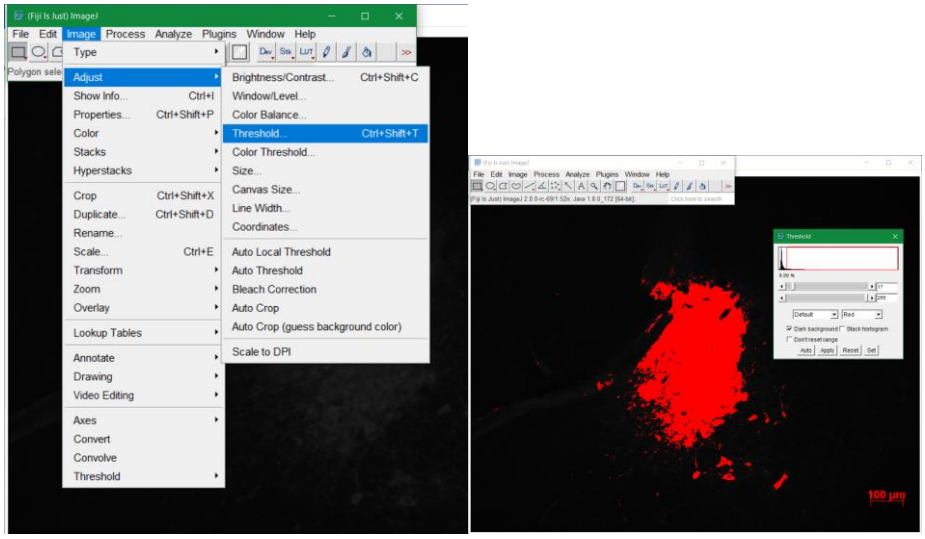

- **Select the threshold value after the peak of low intensity**

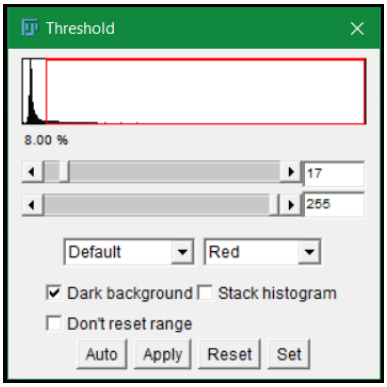

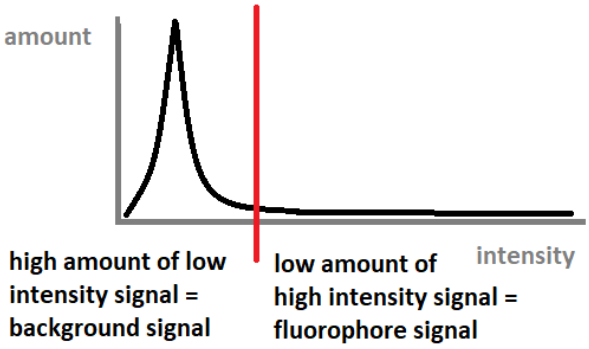

- **Apply this to both the green and red channel**

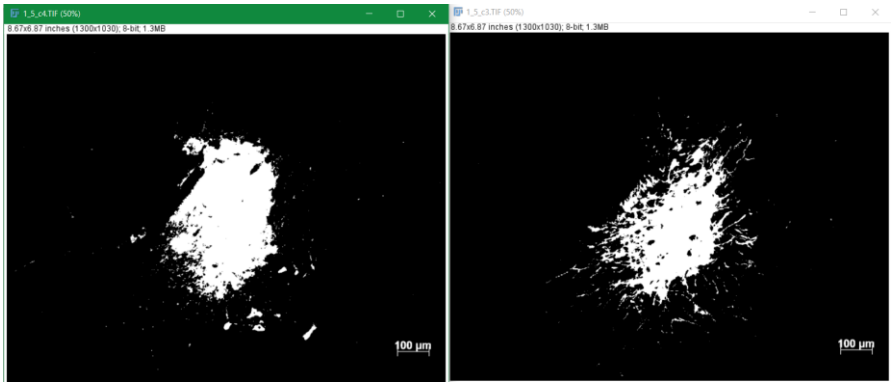

- **Create an inverse selection around the scale bar to exclude these pixels from being counted as well**

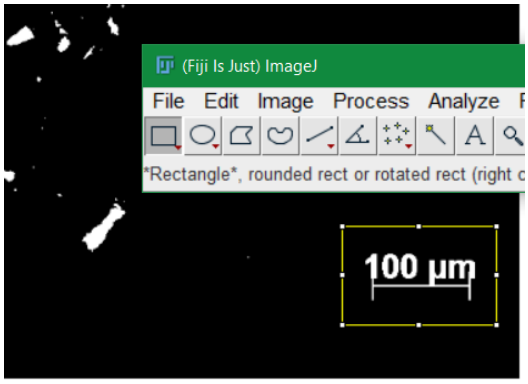

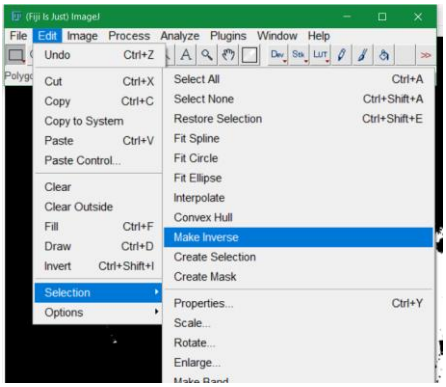

- **Open the *Histogram* function**

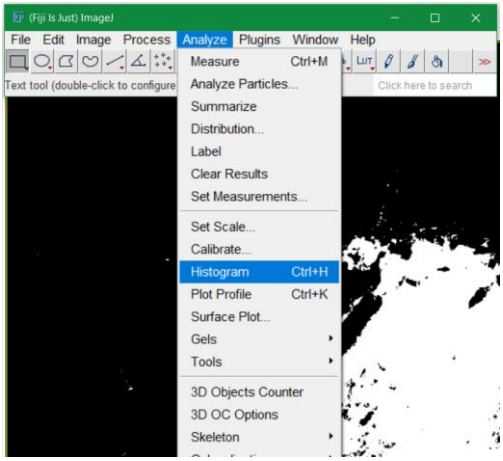

- **Open *List* and note the number of pixels with value 255 (= number of white pixels)**

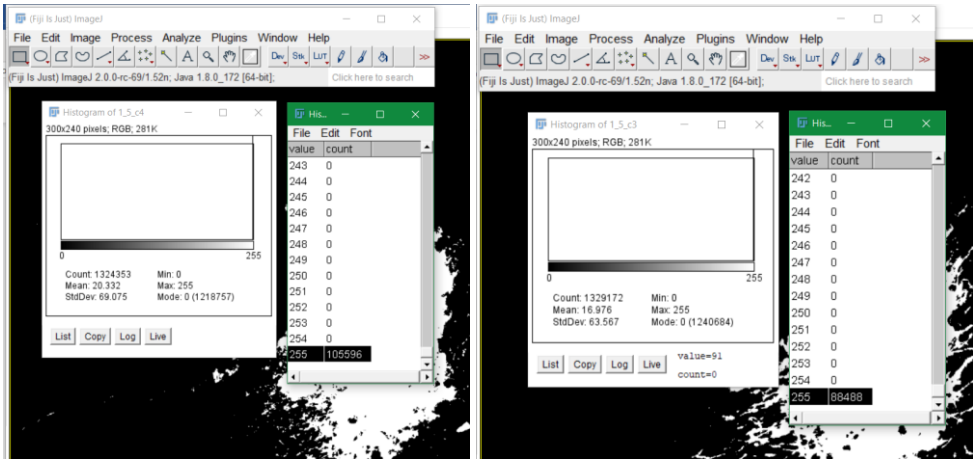

- **Divide the number of white pixels on the red channel by the number of white pixels on the green channel to obtain the red/green ratio**

$$\frac{\#\text{ white pixels red channel}}{\#\text{ white pixels green channel}} * 100 = X\ \%$$

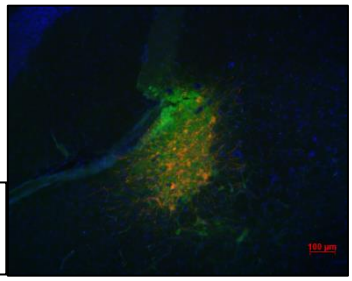

$$\frac{8848}{105596} * 100 = 83{,}798\ \%$$

2. Protocol manual cell counting in ImageJ

- **Create a merged image of the green and blue channels**

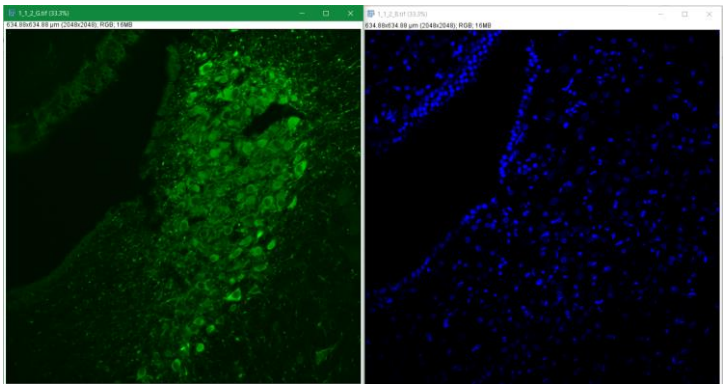

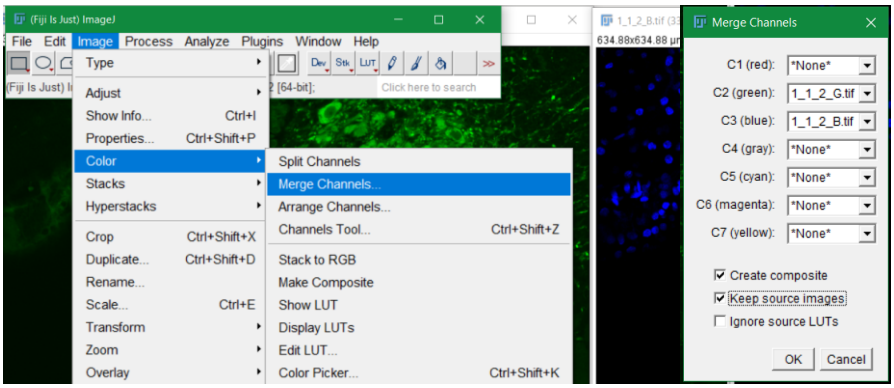

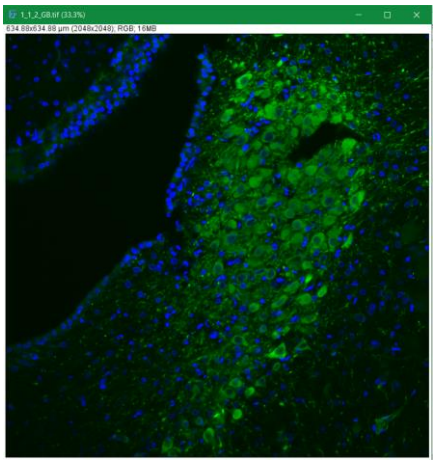

- **Mark all green (TH+) cells with a visible blue nucleus using the multi-point tool**

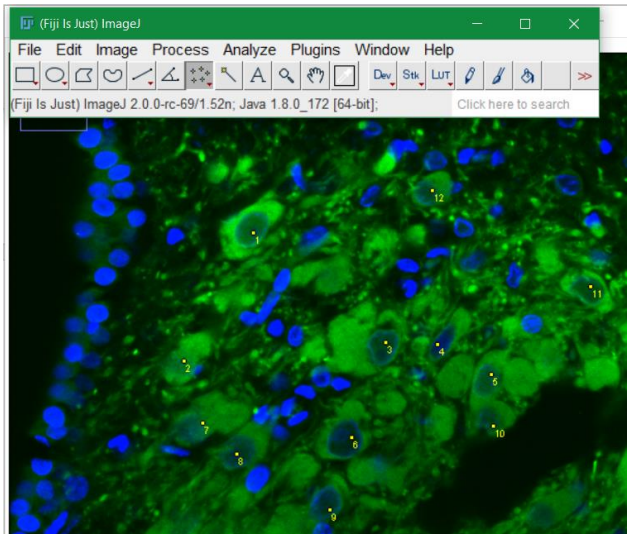

- **Add the markers to the ROI manager**

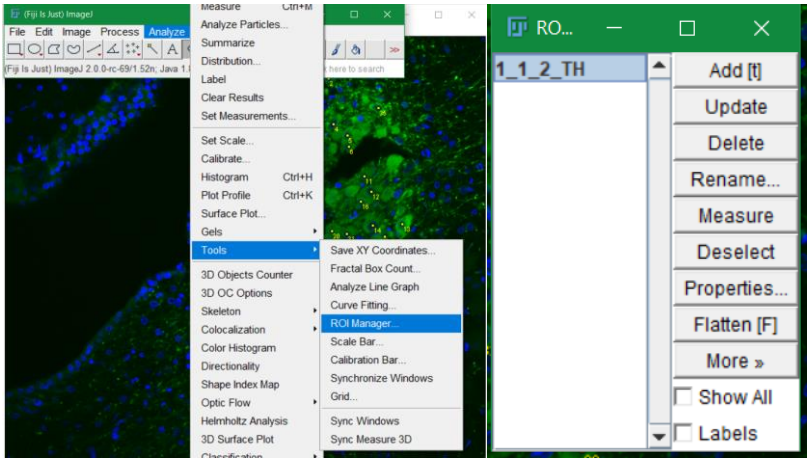

- **Create a merged image of the red and green channels**
- **Apply the markers on the red channel and/or the red+green image by selecting them in the ROI manager**

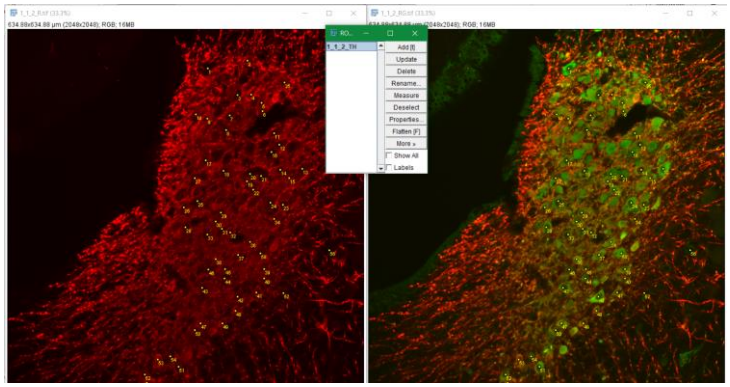

- **Using these images, determine for each marker if the marked cell is double positive (TH+/mCherry+)**

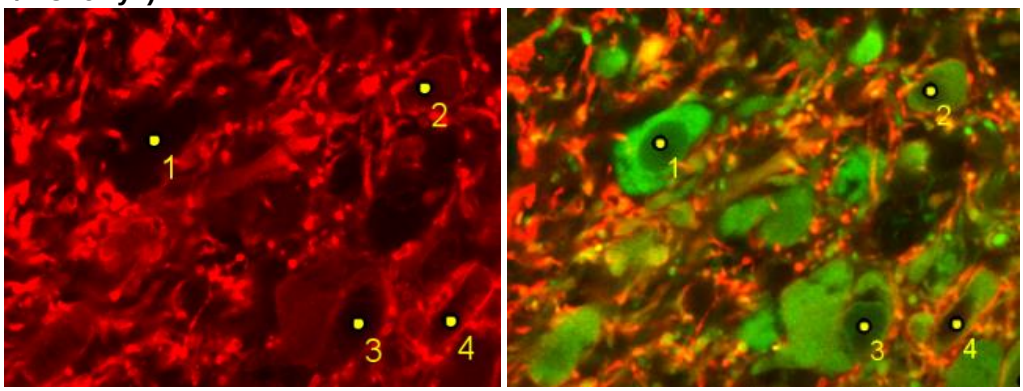

1	**-**
2	**+**
3	**+**
4	**+**

3. Selection of high quality images

Images indicated by a green frame were selected as high quality images.

- **Animal: LSO1**

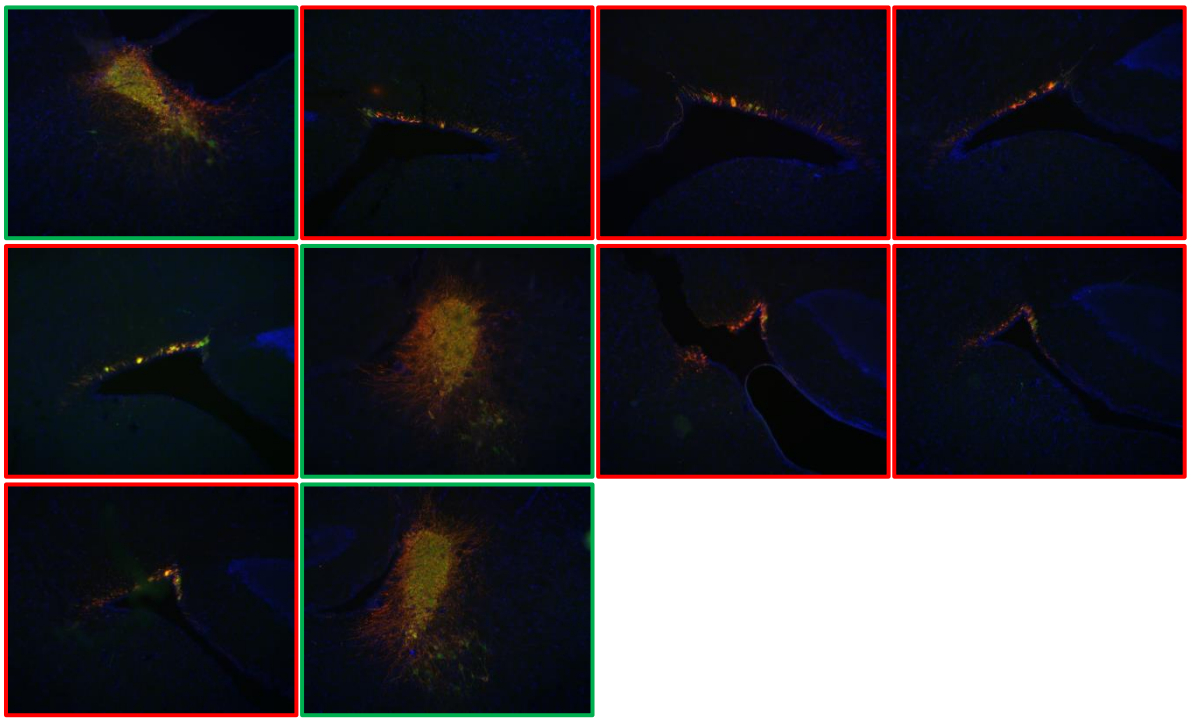

- **Animal: LSO6**

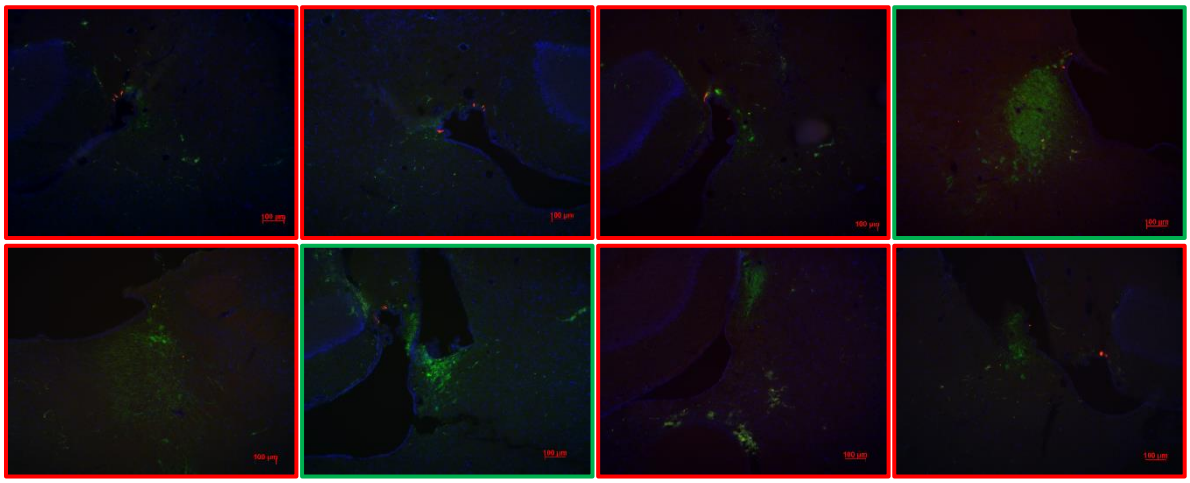

- **Animal: LSO7**

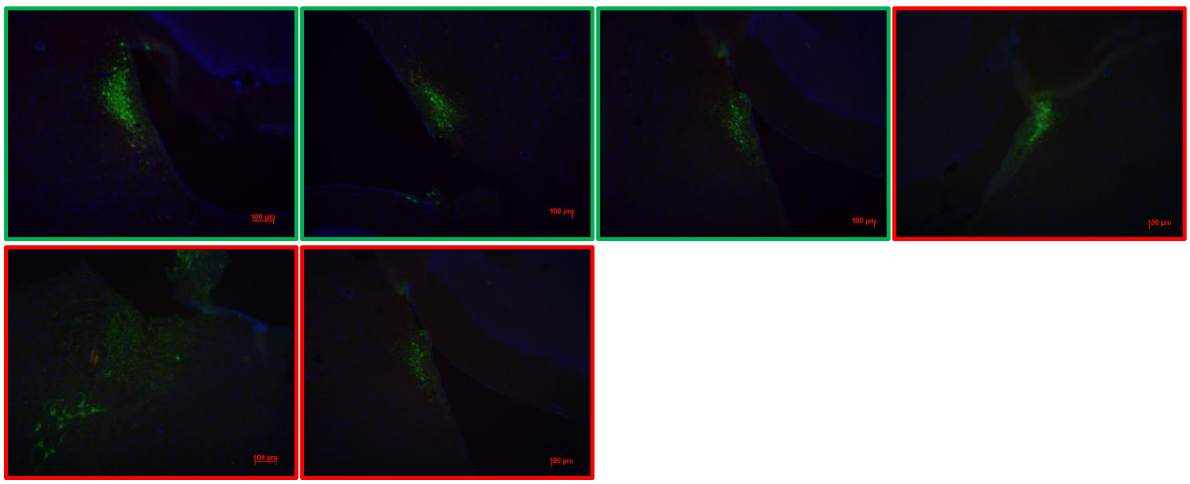

- **Animal: LSO8**

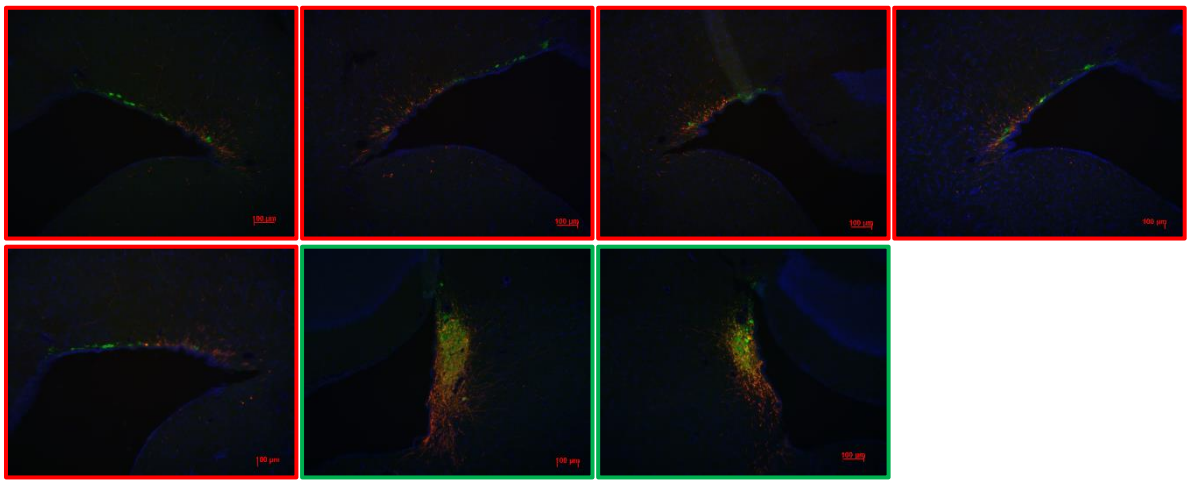

- **Animal: JOEL1**
  - **Left LC**

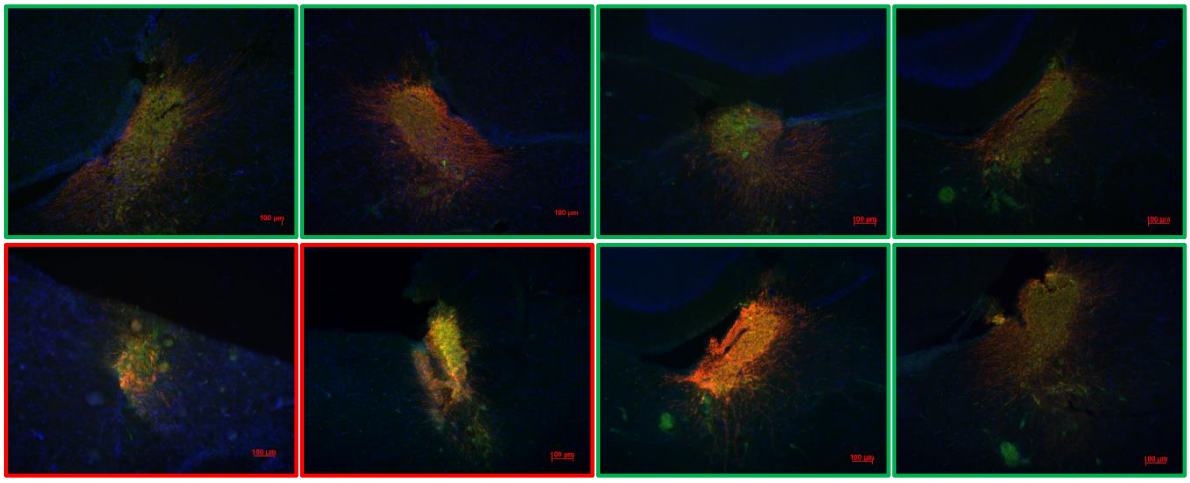

  - **Right LC**

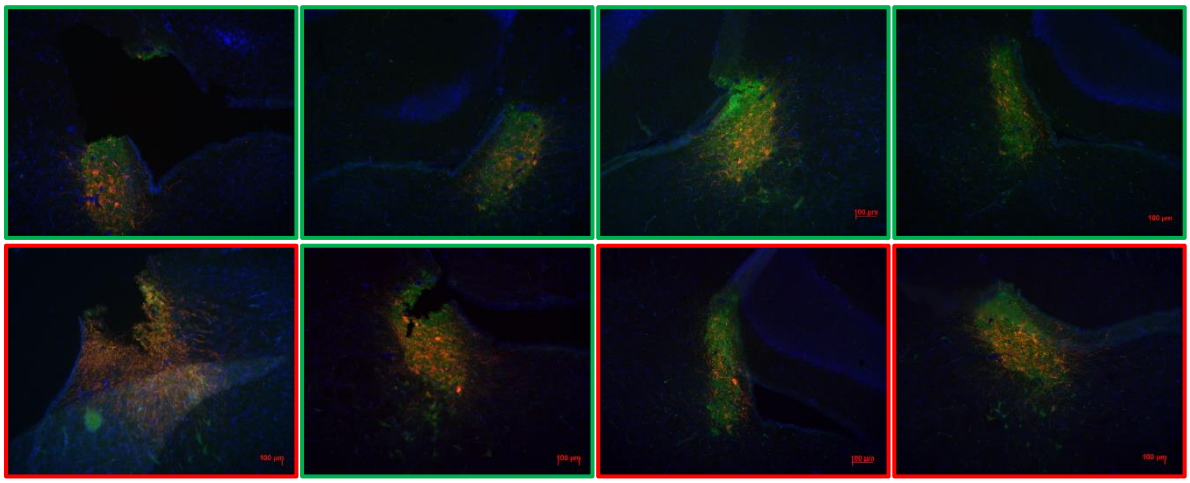

- **Animal: JOEL3**
  - **Left LC**

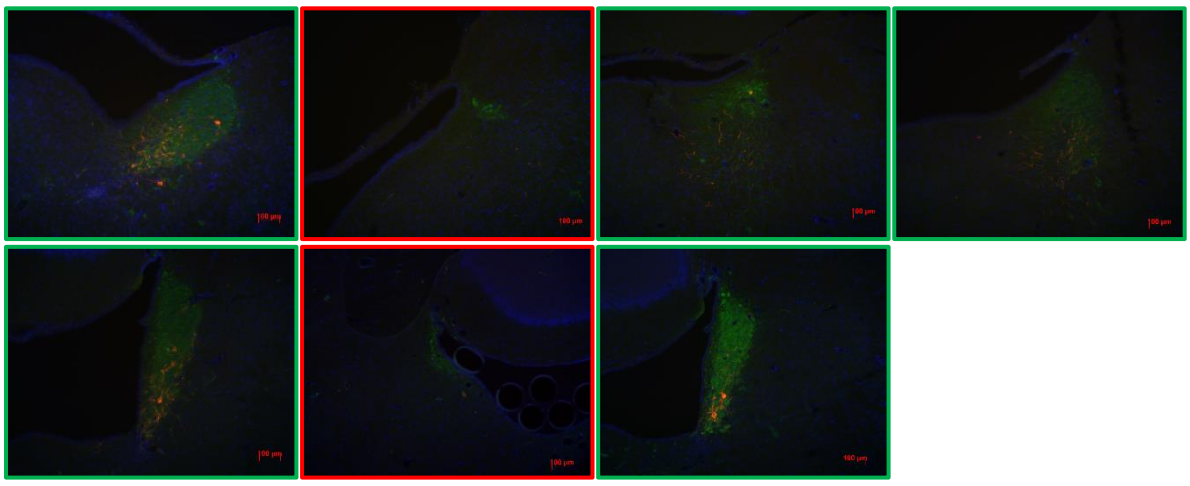

- **Right LC**

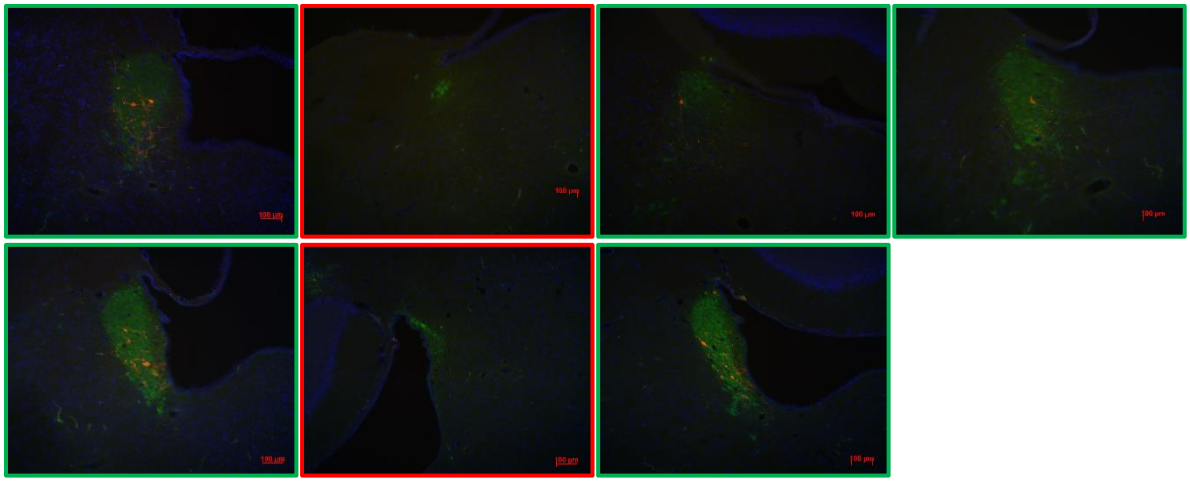

- **Animal: JOEL4**
  - **Left LC**

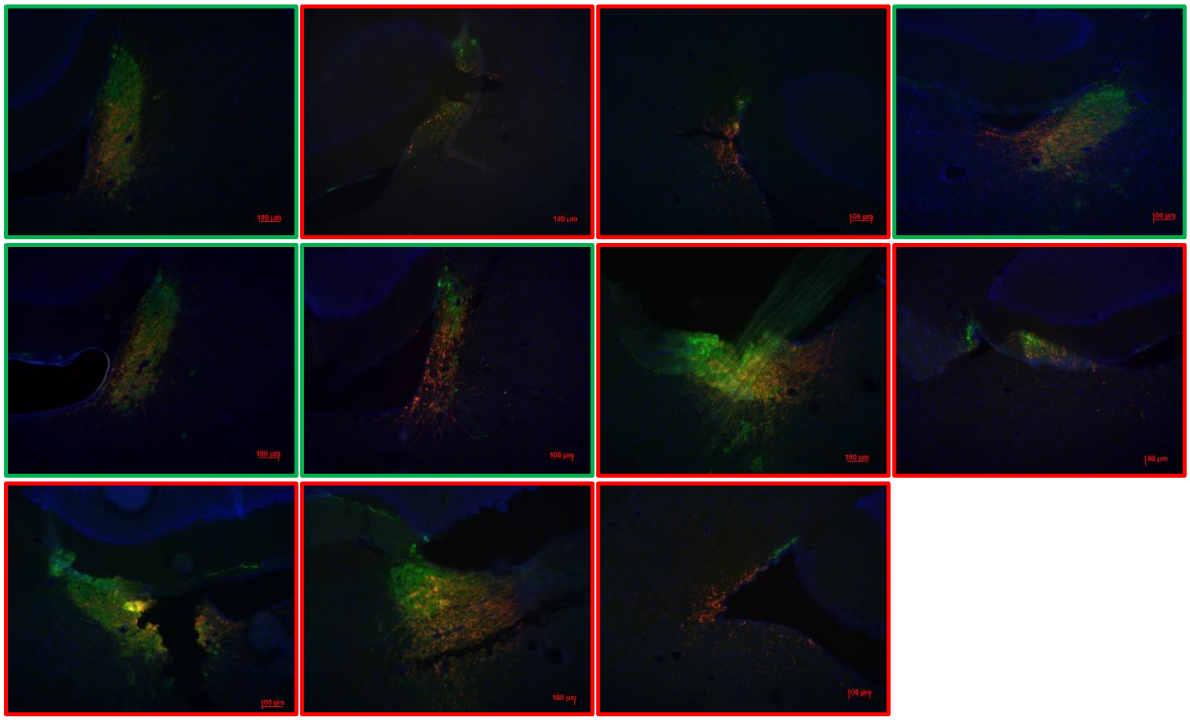

- **Right LC**

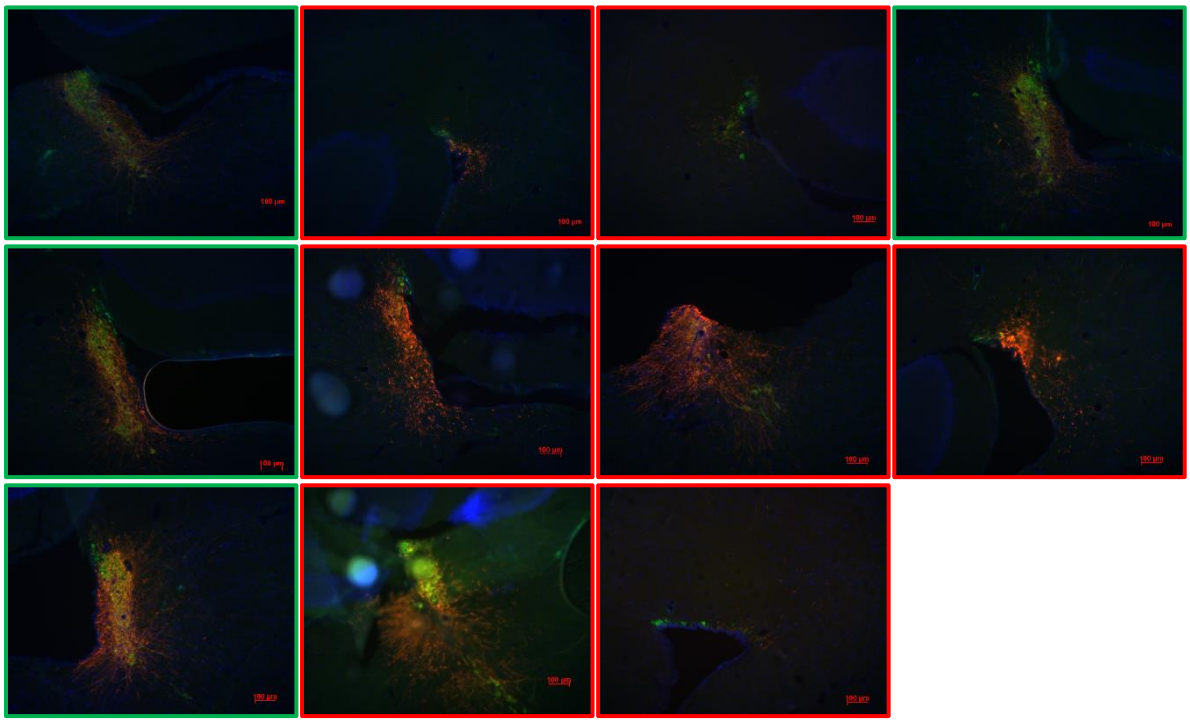

- **Animal: JOEL6**
  - **Left LC**

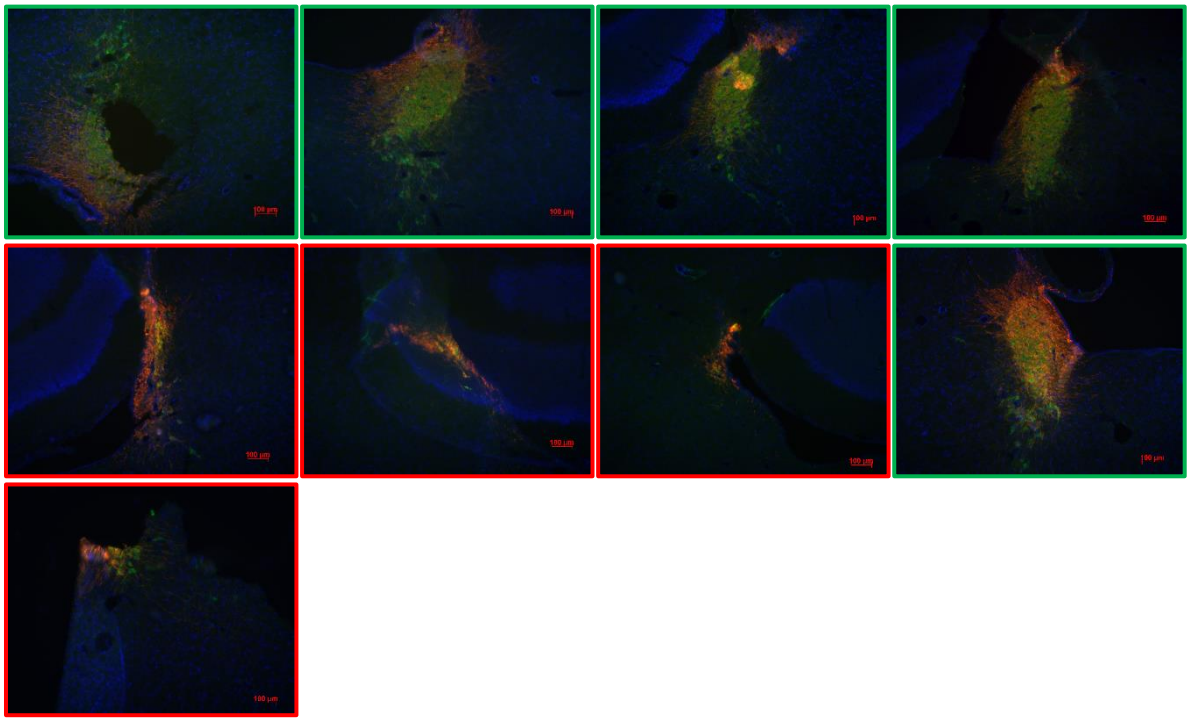

- **Right LC**